iScience

CellPress
OPEN ACCESS

Article

Intra-tumoral YAP and TAZ heterogeneity drives collective NSCLC invasion that is targeted by SUMOylation inhibitor TAK-981

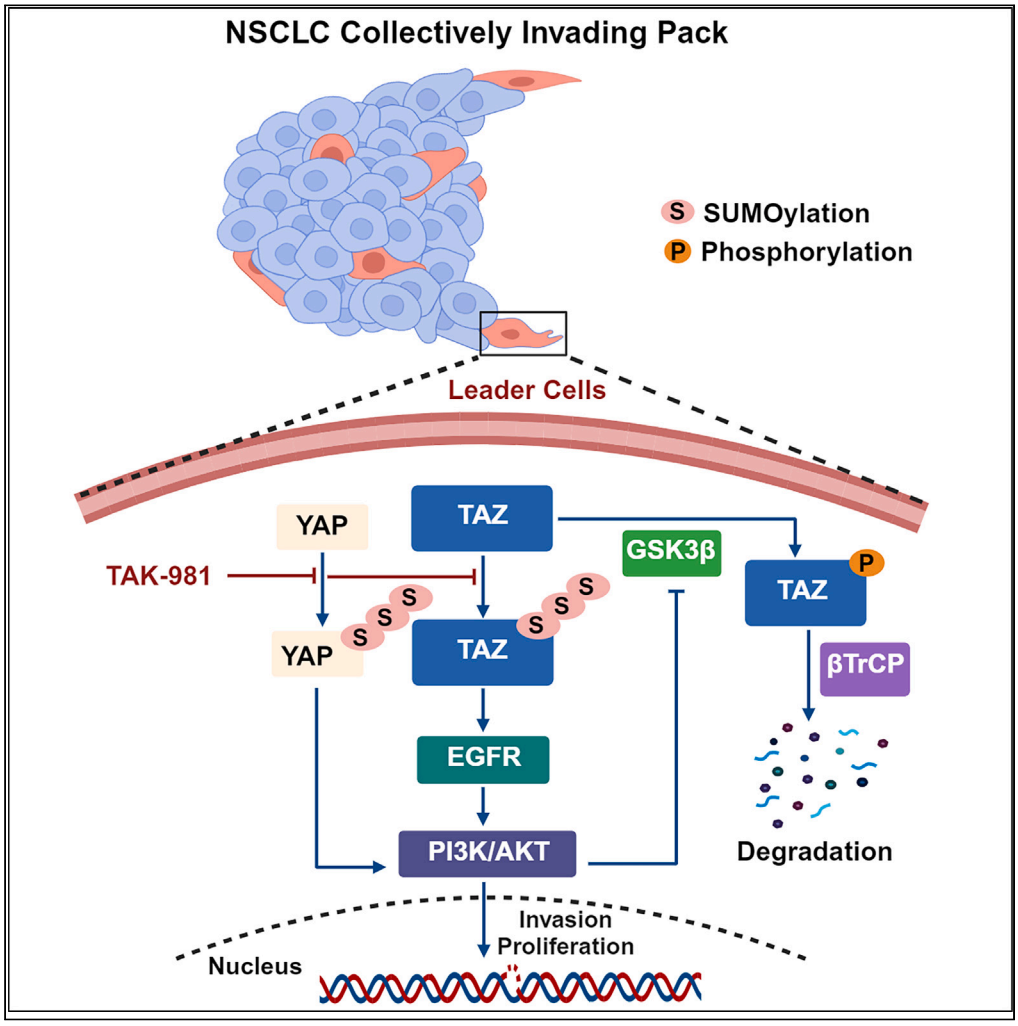

Richa Sharma, Shagun Sharma, Pratik Shriwas, ..., Ticiana Leal, Adam I. Marcus, Mala Shanmugam

mala.shan@emory.edu

Highlights

Leader and follower cells exhibit differential YAP and TAZ dependencies

TAZ-induced invasion in leader cells involves activation of EGFR-PI3K/AKT signaling

Reduced βTrCP in leader cells elevates TAZ expression

TAK-981 suppresses YAP, TAZ, and metastasis in preclinical NSCLC

Sharma et al., iScience 27, 111133
November 15, 2024
https://doi.org/10.1016/j.isci.2024.111133

iScience

CellPress
OPEN ACCESS

Article

Intra-tumoral YAP and TAZ heterogeneity drives collective NSCLC invasion that is targeted by SUMOylation inhibitor TAK-981

Richa Sharma,[1] Shagun Sharma,[1] Pratik Shriwas,[1] Labdhi Mehta,[1] An H. Vu,[1] Janna K. Mouw,[1] Junghui Koo,[1] Chunzi Huang,[1] Veronika Y. Matsuk,[1] Carol Tucker-Burden,[1] Gregory Joseph,[1] Madhusmita Behera,[1] Shi-Yong Sun,[1] Melissa A. Roy,[2] Melissa Gilbert-Ross,[1] Ticiana Leal,[1] Adam I. Marcus,[1] and Mala Shanmugam[1,3,*]

SUMMARY

Non-small cell lung cancer (NSCLC) collective invasion is supported by cooperativity of proliferative (follower) and invasive (leader) cells. H1299-isolated follower cells exhibit higher Yes-associated protein (YAP) expression, while leader cells were found to express elevated transcriptional coactivator with PDZ-binding motif (TAZ/WWTR1) expression. Suppressing TAZ (not YAP) in leader cells reduced invasion. TAZ-regulated leader cell invasion is associated with activation of the EGFR-PI3K-AKT axis. NSCLC patient samples also demonstrated heterogeneity in YAP and TAZ expression. YAP and TAZ regulate proliferation of follower and leader cells. Our results highlight the need to inhibit both YAP and TAZ to effectively target their regulation of collective invasion. We identify that the SUMOylation inhibitor TAK-981 reduces YAP and TAZ expression, decreasing tumor burden and metastasis in a murine NSCLC model. Our study reveals an intra-tumoral division of labor, driven by differential YAP and TAZ expression, which can be effectively targeted with TAK-981 for NSCLC therapy.

INTRODUCTION

Lung cancer remains the leading cause of cancer-related deaths with metastases and the refractory nature of the metastasized cancer contributing to dismal survival rates.[1,2] Eighty-five percent of lung cancers are of the non-small cell lung cancer (NSCLC) subtype that metastasize to the bones, lungs, brain, liver, adrenal glands, and extra thoracic lymph nodes.[3,4] Staging correlates with the extent of metastases, and stage IV NSCLC patients have a 5% survival rate at 5 years compared to a 57% survival rate reported for stage I diagnoses, underscoring the need to prevent and target cancer metastases.[5]

Tumor cells extravasate into surrounding tissues and organs, largely via single cells or collective invasion of packs of cells.[6] Most solid tumors including NSCLC exhibit collective invasion, where groups of tumor cells collectively move as a pack to distant sites. We and others have shown that the cells in these collective packs exhibit phenotypic, genetic, epigenetic, and metabolic heterogeneity that is required to sustain collective invasion.[7–9] Intra-tumoral heterogeneity contributes to differential therapy sensitivity, relapse, and poor clinical outcomes.[10–13] Investigating phenotypically heterogeneous cell populations is hampered by the inability to isolate phenotypically distinct cellular populations. We have taken advantage of pure populations of proliferative "follower" and invasive "leader" NSCLC cells isolated from the collectively invading H1299 cell line isolated using a spatiotemporal genomic and cellular analysis technique.[7] Here, H1299 lung cancer cells were stably transfected with Dendra2, a photoconvertible fluorophore. Invading cells were photoconverted, flow sorted, and expanded, generating pure populations of leader and follower cells.[7] The presence of leader and follower types of cells and division of labor contributing to the progression of disease has also been observed in breast, ovarian, and lung cancers.[14–18] H1299-isolated leader cells (hereafter referred to as leader cells) secrete increased vascular endothelial growth factor (VEGF) that facilitates follower cell recruitment in invasive chains through an atypical VEGF signaling cascade.[7,15] Leader cells also exhibit increased fibronectin synthesis and secretion that activates integrin/focal adhesion kinase (FAK) signaling to promote invasion.[7] Additionally, epigenetic alterations in leader cells were found to increase filopodial motor protein MYO10 expression to alter filopodia dynamics and fibronectin patterning at the edge of 3D collectively invading packs of cells.[19] We previously demonstrated that follower and leader cells exhibit distinct metabolic dependencies that drive proliferation versus invasive states. We found proliferative follower cells exhibit elevated GLUT1 expression and increased glycolysis, while invasive leader cells exhibit a greater dependence on mitochondrial oxidative phosphorylation (OXPHOS) driven by elevated pyruvate dehydrogenase (PDH) activity.[20]

[1]Department of Hematology and Medical Oncology, Winship Cancer Institute, School of Medicine, Emory University, Atlanta, GA, USA
[2]Division of Pathology, Emory National Primate Research Center, Atlanta, GA, USA
[3]Lead contact
*Correspondence: mala.shan@emory.edu
https://doi.org/10.1016/j.isci.2024.111133

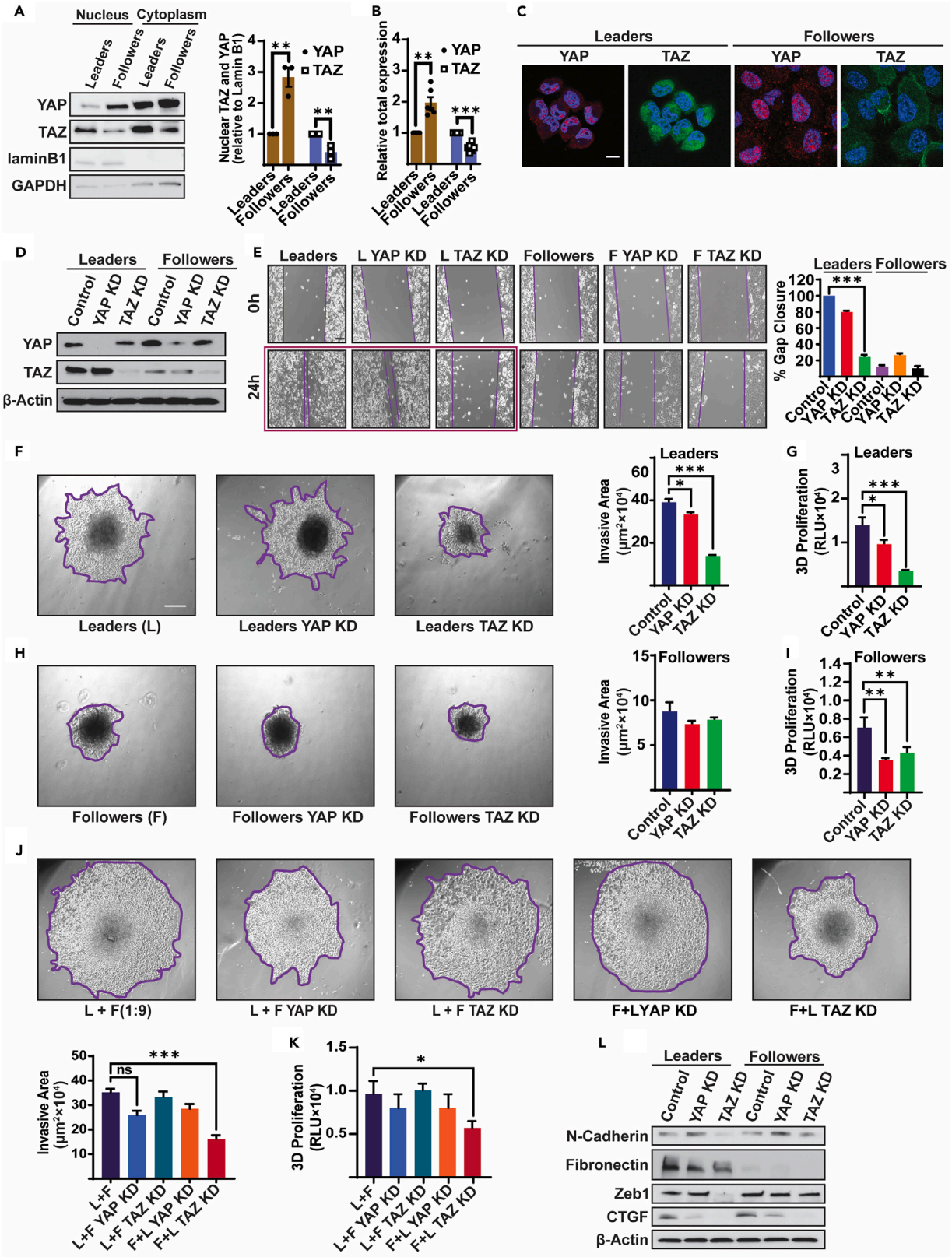
A
Nucleus
Cytoplasm
Leaders
Followers
Leaders
Followers
YAP
TAZ
laminB1
GAPDH
Nuclear TAZ and YAP (relative to Lamin B1)
YAP
TAZ
Leaders
Followers
Leaders
Followers
B
Relative total expression
YAP
TAZ
Leaders
Followers
Leaders
Followers
C
Leaders
Followers
YAP
TAZ
YAP
TAZ
D
Leaders
Followers
Control
YAP KD
TAZ KD
Control
YAP KD
TAZ KD
YAP
TAZ
β-Actin
E
Leaders
L YAP KD
L TAZ KD
Followers
F YAP KD
F TAZ KD
0h
24h
Leaders
Followers
% Gap Closure
Control
YAP KD
TAZ KD
Control
YAP KD
TAZ KD
F
Leaders (L)
Leaders YAP KD
Leaders TAZ KD
Leaders
Invasive Area (μm²×10⁴)
Control
YAP KD
TAZ KD
G
Leaders
3D Proliferation (RLU×10⁴)
Control
YAP KD
TAZ KD
H
Followers (F)
Followers YAP KD
Followers TAZ KD
Followers
Invasive Area (μm²×10⁴)
Control
YAP KD
TAZ KD
I
Followers
3D Proliferation (RLU×10⁴)
Control
YAP KD
TAZ KD
J
L + F(1:9)
L + F YAP KD
L + F TAZ KD
F+LYAP KD
F+L TAZ KD
Invasive Area (μm²×10⁴)
ns
L+F
L+F YAP KD
L+F TAZ KD
F+L YAP KD
F+L TAZ KD
K
3D Proliferation (RLU×10⁴)
L+F
L+F YAP KD
L+F TAZ KD
F+L YAP KD
F+L TAZ KD
L
Leaders
Followers
Control
YAP KD
TAZ KD
Control
YAP KD
TAZ KD
N-Cadherin
Fibronectin
Zeb1
CTGF
β-Actin

Figure 1. YAP and TAZ are differentially expressed in H1299 leader (L) and follower (F) cells, and TAZ regulates leader cell migration and collective invasion with follower cells

(A) YAP and TAZ expression evaluated and quantified in nuclear and cytosolic fractions of leader and follower cells using Lamin B1 and GAPDH as loading controls. Data are mean ± SEM from three independent experiments.

(B) Quantitation of total YAP and TAZ protein levels, normalized to loading control. Data are mean ± SEM from six independent experiments.

(C) Representative immunofluorescence images of endogenous YAP (red) and TAZ (green) merged with nuclear stain DAPI (blue) in leaders and follower cells (scale bar, 10 μm).

(D) YAP and TAZ expression in non-targeting (control) or YAP/TAZ shRNA-transduced leader and follower cells assessed by western blot analysis.

(E) Cells from (D) evaluated for migratory potential in a scratch assay at indicated time points with gap closure quantified relative to respective controls (n = 3; scale bar, 100 μm).

(F–I) Proliferation and invasive potential of spheroids generated from control or YAP or TAZ-KD (F and G) leader cells, (H and I) follower cells, and (J and K) mixes of 10% leader cells with 90% follower cells (L:F, 1:9) assessed for 3D invasive area (n = 4; scale bar, 100 μm).

(L) Expression levels of indicated proteins evaluated in lysates from (B). Representative blots from one of three independent experiments are presented using β-actin as loading control. Data are represented as mean ± SEM. An ordinary one-way ANOVA with a Tukey's multiple comparisons test was used to determine significance compared to control or as indicated. *$p < 0.05$, **$p < 0.01$ ***$p < 0.001$ compared to the indicated group in *post hoc* tests.

Elucidating the mechanistic basis and factors necessary for maintaining phenotypic heterogeneity and collective cell invasion can reveal newer methods to target collective cell invasion. The individual cells within an invading pack are subject to different mechanical and extrinsic environmental conditions. One central pathway responsive to mechanical stress is the Hippo signaling pathway comprising the highly conserved large tumor suppressor (LATS1/2) and MST1/2 kinases.[21] Hippo signaling engages downstream transcription factors Yes-associated protein (YAP) and transcriptional coactivator with PDZ-binding motif (TAZ, also called WWTR1) that, with specific co-activators, play central roles in the growth of embryonic tissues, wound healing, and organ regeneration.[22] A wide variety of human malignancies exhibit hyperactivation of YAP and TAZ.[23] Despite playing complementary roles, YAP and TAZ activate distinct transcriptional signatures. YAP promotes metastatic signaling in triple-negative breast cancer, melanoma, and NSCLC.[24–26] On the other hand, TAZ is hyperactivated in papillary thyroid carcinoma, Ewing sarcoma, breast cancer, and NSCLC leading to epithelial-to-mesenchymal transition (EMT) and increased invasion.[27,28] YAP has been reported to preferentially regulate cell proliferation and cell-cycle progression, whereas TAZ regulates cell adhesion and cell migration.[29] Nevertheless, the functional implications of the non-overlapping biology they regulate in collective invasion remain underexplored.

In this study, we took advantage of proliferative follower and invasive leader cells to investigate whether YAP and TAZ contribute to their distinct phenotypes and collective invasion. We found follower cells exhibit higher expression and nuclear localization of YAP in contrast to the leader cells that exhibit higher expression and nuclear localization of TAZ. TAZ was found to be necessary for maintaining the invasiveness of leader cells through EGFR-PI3K/AKT signaling. Elevated YAP expression in follower cells maintained their proliferation. The heterogeneity in YAP and TAZ expression was necessary to sustain the phenotypic heterogeneity in collectively invading NSCLC.

Historically, targeting the YAP/TEA domain (TEAD) interaction has been thought to be fundamental in cancer therapy, with less emphasis on targeting TAZ-driven biology. Our studies thus provide the impetus for therapeutic targeting of both YAP and TAZ in NSCLC. In investigating the basis for differential YAP/TAZ expression in leader cells and follower cells, we found the E3 ubiquitin (Ub) ligase βTrCP to play a central role in regulating TAZ stability, leading to increased expression of TAZ in leader vs. follower cells. Our studies reveal the utility of the small ubiquitin-like modifier (SUMO) inhibitor TAK-981 in reducing both YAP and TAZ expression and its preclinical utility in NSCLC.

RESULTS

YAP and TAZ are differentially expressed in H1299-derived leader and follower cells and uniquely support invasion vs. proliferation

Hippo signaling effectors YAP and TAZ are known to play a central role in promoting tumor growth and metastases.[30] Given the previously established phenotype of H1299 leader cells as highly invasive in contrast to follower cells as highly proliferative,[31] we investigated a role for YAP and TAZ in supporting these distinct phenotypes. We found follower cells exhibited higher expression of YAP while leader cells exhibited elevated expression of TAZ. (Figures 1B and 1D). Since the effector activities of YAP and TAZ depend on their nuclear translocation, we evaluated their nuclear abundance in leader and follower cells. We found higher nuclear TAZ vs. YAP in leader cells and higher nuclear YAP vs. TAZ in follower cells (Figures 1A and 1C). To investigate whether differential YAP and TAZ expression contributes to the distinct invasive vs. proliferative phenotypes, we generated YAP/TAZ knockdown (KD) of leader and follower cells (KD efficiency for two different short hairpin RNAs (shRNAs) is shown in Figures 1D and S1). We interrogated the effects of YAP or TAZ KD on proliferation, migration, and 3D spheroid invasion (Figure 1D). The impact of YAP or TAZ KD on the migratory capacity of leader and follower cells was examined using a wound healing scratch assay. Leader TAZ-KD cells exhibited significantly reduced migratory potential as compared to leader YAP-KD cells (Figure 1E). Follower cells do not migrate, and, as anticipated, neither YAP nor TAZ suppression altered their migratory capacity (Figure 1E). Leaders are positioned at the leading edge of the collectively invading pack and are required for the collective migration of the pack, as a whole.[31] We therefore investigated the effects of YAP and TAZ KD on invasion and proliferation in 3D cultures, in which leader cells mixed with follower cells, in a previously optimized (1:9) ratio,[31] cooperate to collectively invade. Both YAP and TAZ KD in leader cells inhibited their 3D invasion and proliferation (Figures 1F and 1G) with no effect noted in follower cell invasion with YAP or TAZ KD although there was a significant decrease in their 3D proliferation (Figures 1H and 1I). We found significant suppression of collective invasion and proliferation of leaders with TAZ KD vs. leader YAP-KD cells in the follower-leader mixture invasion assays (Figures 1J and 1K). Neither YAP nor TAZ KD of follower cells

impacted the 3D invasive potential of the corresponding follower-leader mixes (Figures 1J and 1K). Collective invasion occurrence in 3D culture was verified by demonstrating N-cadherin expression, a key regulator of collective cell migration, at adherens junctions in a pack of invading parental H1299 cells (Figure S1E). Evaluation of TAZ and YAP expression in collectively invading spheroids qualitatively demonstrates increased TAZ in leading vs. trailing cells of the collective pack and, in contrast, elevated YAP in cells interior of the spheroid vs. the cells at the leading edges (Figure S1E).

To start to understand the mechanistic basis for TAZ selectively regulating invasion, we queried leader and follower YAP/TAZ-KD cells for regulation of proteins canonically associated with migration/invasion. In leader cells, TAZ KD reduced expression of N-cadherin, fibronectin, Zeb1, and connective tissue growth factor (CTGF) gene while KD of YAP suppressed CTGF expression. Fibronectin and CTGF levels were also downregulated in follower YAP- and TAZ-KD cells (Figure 1L). Lastly, we previously reported leader cells exhibit increased dependence on OXPHOS that is required to maintain invasiveness.[20] We therefore tested the effects of YAP/TAZ KD on follower and leader cell OXPHOS capacity and found leader cells to exhibit reduced oxygen consumption rate and coupled respiration upon TAZ vs. YAP KD (Figure S2). Overexpression of TAZ but not YAP significantly increased the invasive potential of leader cells; however, YAP or TAZ overexpression did not increase follower cell invasive potential (Figure S3). Our findings, in sum, reveal differential expression of YAP and TAZ in proliferative vs. invasive cells, and non-redundant roles for YAP and TAZ that support collective invasion.

YAP and TAZ exhibit intra-tumoral heterogeneity in human NSCLC metastases, and TAZ expression positively correlates with fibronectin expression in human NSCLC

To further investigate the clinical relevance of YAP and TAZ, we examined their protein expression in human lung cancer tumor metastases. Both YAP and TAZ were found to exhibit heterogeneity in intra-tumoral expression patterns (Figure 2A). Since we do not have leader or follower markers, the cellular quantification of YAP/TAZ could not be performed in these samples; however, these results underscore a potential role for differential expression of YAP and TAZ within a tumor. Since fibronectin is highly expressed in leader cells as compared to follower cells,[19] despite it also being a secreted protein, we used fibronectin as a proxy to correlate with biology related to leader types of cells in tumor samples. Interrogating the cancer genome atlas (TCGA)-Broad Institute Firehose lung adenocarcinoma (LUAD) dataset, we showed a significant correlation between fibronectin and TAZ levels, which was not detected between fibronectin and YAP expression (Figure 2B).

TAZ increases EGFR expression in leader cells

Expression of EGFR mutants and/or increased expression of EGFR are known to correlate with aggressive metastatic NSCLC.[32] EGFR regulates Hippo signaling in a feedforward loop.[33–36] We therefore investigated the relationship of YAP/TAZ and EGFR expression in follower and leader cells and queried our institutional dataset (Winship molecular profiling study 2020) for YAP and TAZ mRNA expression and its correlation with EGFR mRNA. Our data show a positive correlation of both YAP and TAZ mRNA with EGFR mRNA expression (Figure 3A). Investigation of the levels of EGFR protein in leader and follower cells, interestingly, revealed higher EGFR protein expression in leader compared to follower cells, correlating with TAZ expression (Figures 3B and 3D). TAZ KD, unlike YAP KD, suppressed EGFR expression in leader cells with no effect noted in follower cells that basally express low levels of EGFR (Figure 3B). Next, to test the sufficiency of TAZ in inducing EGFR expression, we overexpressed TAZ or YAP in TAZ-KD leader cells and evaluated EGFR expression. Overexpression of TAZ in TAZ-KD leader cells increased EGFR protein and mRNA expression (Figures 3C and 3D). YAP overexpression however did not increase EGFR expression in TAZ-KD leader cells (Figure 3D) to the same extent as TAZ overexpression in leader cells. We additionally tested the effects of pharmacological inhibition of EGFR on YAP and TAZ expression. The effects of erlotinib on EGFR inhibition were confirmed by demonstrating a dose-dependent reduction of pAKT in leaders and not in follower cells (Figure 3E). Erlotinib reduced leader cell migration in a scratch assay (Figure S4C) and in a 3D invasion assay of leader cells and mixtures of leader and follower cells in a dose-dependent manner correlating with decrease in 3D proliferation (Figures 3F and 3G), consistent with EGFR being upstream of TAZ. No effects of erlotinib were detected on follower cell migration and invasion, as anticipated, yet their 3D proliferation was significantly reduced (Figures S4C and 3F). Additionally, erlotinib treatment significantly reduced invasive markers fibronectin, N-cadherin, vimentin, and Zeb1 only in leader cells in a dose-dependent manner, phenocopying TAZ KD effects (Figure S4B). EGFR stimulation increased pAKT and TAZ levels, supportive of EGFR being upstream of TAZ (regulating TAZ stability via AKT/GSK3b) (Figure S11). Lastly, TAZ-overexpressing leader cells were insensitive to erlotinib treatment, suggesting EGFR is upstream of TAZ (Figure S10). These results, in sum, demonstrate that TAZ and EGFR regulate their expression reciprocally and support leader cell migration and invasiveness.

TAZ-regulated migration involves the PI3K/AKT axis

EGFR canonically engages the PI3K-AKT-mTOR axis and/or Ras-Raf-MAPK or extracellular signal-regulated kinases (ERK) signaling axis.[37] We examined pERK1/2 in both YAP- and TAZ-KD leader cells and follower cells and found no alteration in pERK levels (Figure S5). We therefore queried the role of the PI3K/AKT axis in mediating the distinct YAP/TAZ-driven effects in follower and leader cells. Concordant with elevated EGFR expression, leader cells also demonstrated higher basal levels of pAKT and pS6 (Figure 4A). YAP and TAZ KD suppressed pAKT and pS6 expression only in leader cells (Figure 4A). Overexpression of YAP or TAZ in leader cells exhibiting TAZ KD restored pAKT and pS6 (Figure 4B). To further query the role of AKT in TAZ-mediated regulation of invasion in leader cells, we overexpressed constitutively active HA-AKT1 or FLAG-AKT2 in leader TAZ-KD cells and evaluated the invasive potential and proliferation of their spheroids. Overexpression of AKT1 and 2 in TAZ-KD leader cells rescued invasion and proliferation in leader TAZ-KD cells and rescued the suppressed collective invasion and proliferation of TAZ-KD leader cells mixed with follower cells (Figures 4C–4F). Both AKT1 and 2

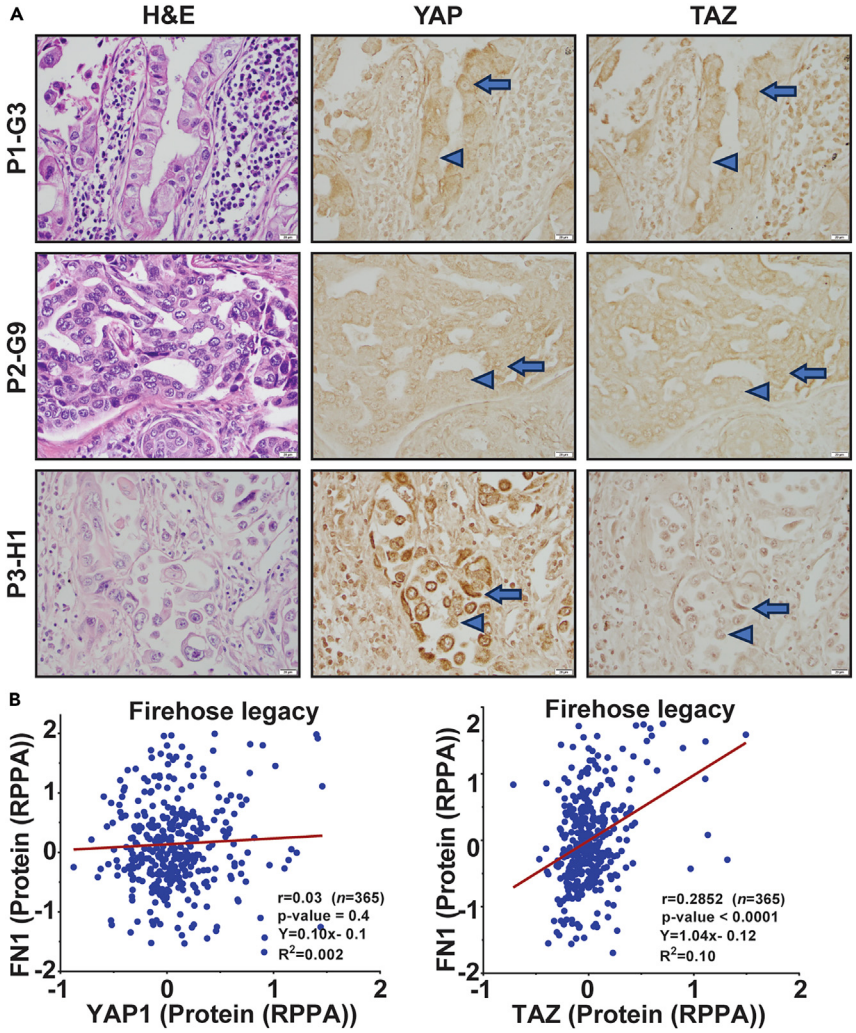

Figure 2. YAP and TAZ exhibit intra-tumoral heterogeneity in NSCLC metastases, and TAZ expression correlates with fibronectin expression in NSCLC

(A) Representative IHC images of YAP and TAZ, from 3 metastatic human non-small cell lung cancer samples. Arrows show neoplastic cells with more intense staining. Arrowheads show neoplastic cells with minimal to no staining. Scale bar, 20 μm.

(B) Correlation analysis of the TCGA-Broad institute (Firehose LUAD dataset) cohort (n = 365) for fibronectin protein with YAP or TAZ expression. A Spearman correlation of 0.2852 (****) and 0.03 (not significant) was determined for TAZ and YAP association with FN, respectively.

overexpression did not increase follower cell invasive potential (Figure S6). These results importantly identify a role for AKT1/AKT2 downstream of TAZ in leader cell invasion (Figures 4C and 4E).

Increased βTrCP expression contributes to reduced TAZ expression in follower vs. leader cells

We next examined the basis of differential YAP/TAZ expression in follower and leader cells. YAP mRNA expression was higher in follower vs. leader cells corresponding with elevated YAP protein expression (Figures 5A and 5B). Interestingly, TAZ mRNA levels were comparable in follower and leader cells (Figure 5A). We next tested whether altered TAZ protein stability accounted for differential TAZ protein expression. Treatment of leader and follower cells with the proteasome inhibitor MG132 increased TAZ expression in follower cells, suggesting reduced TAZ stability in follower vs. leader cells (Figure 5B). Glycogen synthase kinase 3 (GSK3) phosphorylates the N-terminal phosphodegron in TAZ, increasing its binding to the Skp1-Cullin-F-box (SCF)$^{\beta TrCP}$ subunit of E3 Ub ligase, βTrCP, leading to TAZ ubiquitylation and degradation.[38] GSK3 activity is suppressed by AKT phosphorylating serine 9 in GSK3β.[39] We found leader cells exhibited higher GSK3β phosphorylation than follower cells that correlated with their elevated pAKT expression (Figure 5C). Since GSK3β is inhibited by AKT, we tested the effects of AKT inhibition on YAP and TAZ expression. Supportively, we detected suppression of pGSK3β upon AKT inhibition that corresponded with a reduction of TAZ protein expression in leader cells (Figure 5D). AKT inhibition in follower cells did not impact pGSK and downstream TAZ levels (Figure 5D).

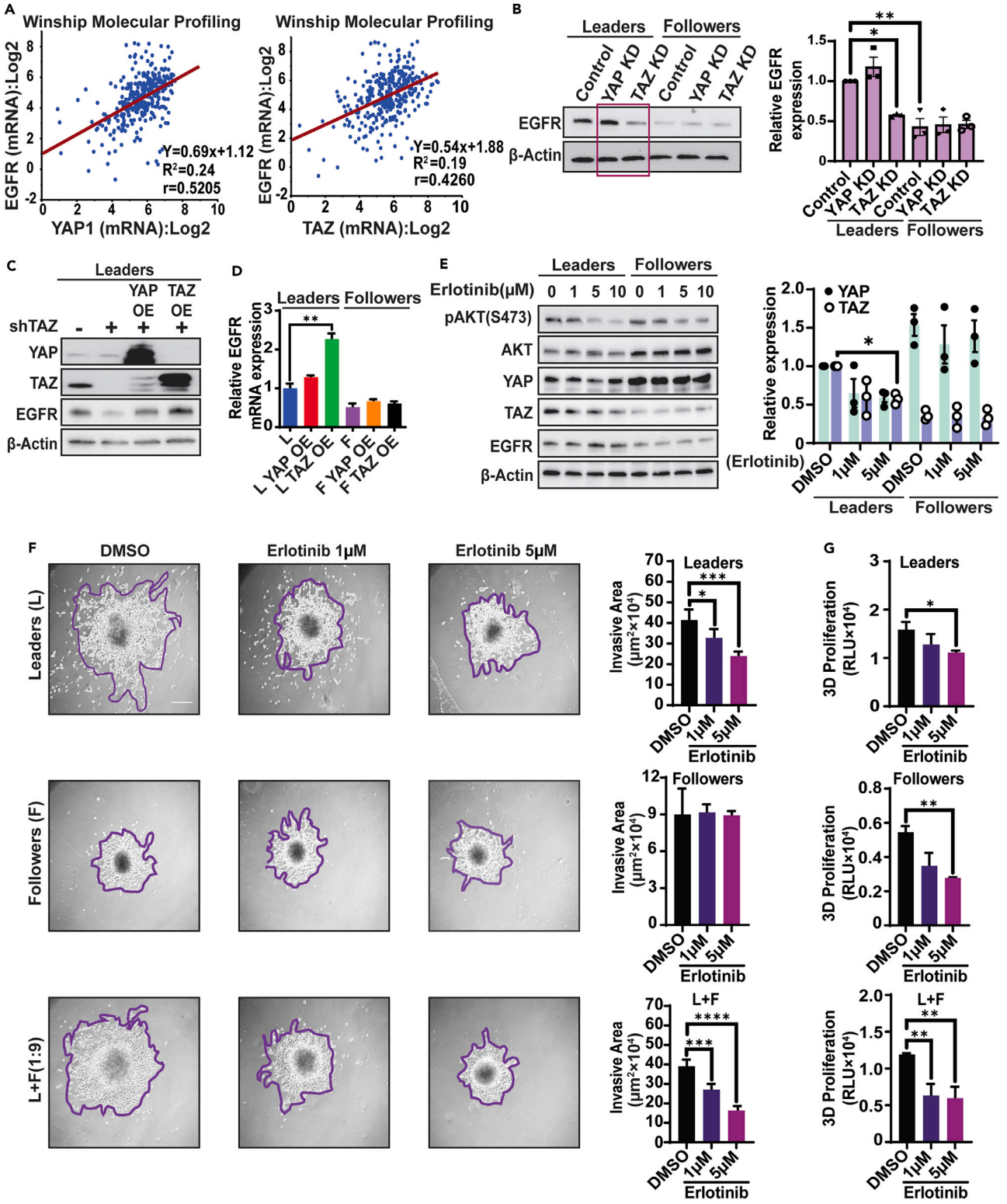

Figure 3. TAZ and EGFR are reciprocally regulated in leader cells

(A) Correlation analysis of EGFR mRNA and YAP and TAZ mRNA expression in our institutional Winship molecular profiling (2020) dataset. A Spearman correlation of 0.4260 (****) and 0.5205 (****) for TAZ and YAP, respectively, vs. EGFR expression was noted (*n* = 343).

Figure 3. *Continued*

(B) Whole cell lysate of leader and follower non-targeting (control) or YAP/TAZ-KD cells from Figure 1B evaluated for EGFR expression. Data are mean ± SEM from three independent experiments.

(C) Whole cell lysates of leader cells, leader TAZ-KD cells, or L TAZ-KD cells overexpressing (OE) YAP or TAZ were evaluated for indicated proteins. Representative blots from one of three independent experiments presented.

(D) EGFR mRNA expression in YAP or TAZ OE leader and follower cells.

(E) Examination of the effect of erlotinib (72 h treatment at indicated doses) on indicated proteins isolated from whole cell lysates of leader and follower cells. Quantitation of the immunoblot analyses (F) for YAP and TAZ, normalized to the loading control. Densitometric quantification from $n = 3$ blots represented as mean ± SEM.

(F and G) Effect of erlotinib on invasive potential and proliferation of spheroids generated with leader cells, follower cells, or 90% follower and 10% leader cells mixes (L: F, 1:9.) with the quantification of invasive area. ($n = 4$; scale bar, 100 μm). Data are represented as mean ± SEM. An ordinary one-way or two-way ANOVA with a Tukey's multiple comparisons test was used to determine significance compared to control or as indicated. *$p < 0.05$, **$p < 0.01$, ***$p < 0.001$, ****$p < 0.0001$ compared to the indicated group.

E3 Ub ligases play a central role in transferring Ub to target proteins, catalyzing the initial steps of protein degradation. We found increased expression of βTrCP in follower vs. leader cells (Figure 5C). βTrCP overexpression reduced YAP and TAZ expression in leader and follower cells, supporting its central role in contributing to differential YAP and TAZ expression in follower and leader cells (Figure 5E). βTrCP KD led to an increase in TAZ expression in follower cells (Figure 5F). While E3 Ub ligases exhibit substrate specificity, each target protein may be regulated by multiple E3 Ub ligases. To identify additional E3 Ub ligases that may account for differential TAZ stability, we queried their expression in follower and leader RNA sequencing (RNA-seq).[19] Several E3 Ub ligases were found to exhibit higher expression in follower vs. leader cells (Figures S7A and S7B). We hypothesized that KD of these E3 Ub ligases would also rescue TAZ degradation and restore TAZ levels in follower cells. As predicted, we detected an increase in TAZ levels in follower vs. leader cells upon KD of E3 Ub ligases like Smurf2, MARCH4, and TRIM38 that exhibited elevated expression in follower cells (Figures S7C and S7D). Overall, these findings suggest that increased PI3K/AKT signaling in leader cells inhibits GSK3, protecting TAZ from degradation by downstream E3 Ub ligases as outlined in schematic Figure 5G.

SUMOylation inhibitor TAK-981 targets YAP and TAZ expression and suppresses collective invasion

Our studies demonstrate distinct signaling regulated by YAP and TAZ promoting follower cell proliferation vs. leader cell invasion. The necessity for both phenotypes in collective invasion underscores the need to target both YAP and TAZ in NSCLC. Verteporfin (VP) is an Food and Drug Administration-approved drug that targets YAP/TEAD interactions.[40,41] We therefore tested the effects of VP on YAP and TAZ expression in follower and leader cells. VP suppressed YAP, TAZ, TEAD, and pAKT only in follower cells with no effect in leader cells (Figure S8A). Leader cell migration was unchanged following VP treatment (Figure S8B). Likewise, in 3D cultures of leader cells, follower cells, and leader and follower cell mixes, VP did not impact invasion and proliferation (Figure S8C). In conclusion, our data underscore the need to target both YAP and TAZ to suppress collective invasion and suggest that agents like VP do not effectively target the distinct biology sustained by both YAP and TAZ.

Given our results showing the large number of E3 Ub ligases capable of regulating YAP and TAZ and the need to increase ubiquitination to suppress protein expression, targeting E3 Ub ligases did not seem to be a plausible approach for targeting both YAP and TAZ expression. In contrast to ubiquitination, SUMOylation of proteins promotes stability.[42] Previous studies have demonstrated YAP SUMOylation and hypothesized that TAZ is SUMOylated and that YAP and TAZ's SUMOylation promotes their stability by preventing their ubiquitination.[43] Therefore, we hypothesized that inhibiting SUMOylation of YAP and TAZ would be an effective method to target their expression.

Subasumstat (TAK-981) is a SUMO inhibitor currently in phase 1 clinical trials for the treatment of non-Hodgkin's lymphomas, multiple myeloma, and advanced or metastatic solid tumors (NCT03648372, NCT04074330, NCT04776018, and NCT04381650). TAK-981 treatment of leader and follower cells reduced both YAP and TAZ expression in a dose-dependent manner, with leader cells showing increased reduction of both YAP and TAZ at lower doses (Figure 6A). Co-treatment with TAK-981 and translation inhibitor cycloheximide further reduced YAP and TAZ expression, and TAK-981 treatment had no effect on the mRNA expression of YAP and TAZ in leader and follower cells (Figures S9C and S9E), suggesting TAK-981 reduction of YAP and TAZ expression occurs via reduction of protein stability (Figure S9C). To confirm that TAK-981 targets the SUMOylation of YAP and TAZ, we analyzed YAP and TAZ immunoprecipitates for basal SUMOylation and the effect of TAK-981 on SUMOylation. We demonstrated SUMOylation of YAP and report SUMOylation of TAZ. SUMOylation of immunoprecipitated TAZ was found to be higher in leader vs. follower cells, and both SUMOylated YAP and TAZ were reduced upon TAK-981 treatment (Figure 6B). The leader cells, interestingly, were more sensitive to TAK-981-induced suppression of YAP and TAZ expression (Figure 6A), corresponding with their elevated SUMOylation. This is a new report of a small-molecule SUMOylation inhibitor to target both YAP and TAZ expression.

We next analyzed the effect of TAK-981 on invasive markers and representative proteins of the EGFR-PI3K/AKT pathway in leader and follower cells. TAK-981 reduced the expression of EGFR, pS6 and pAKT, CTGF, and other proteins involved in metastases such as fibronectin, N-cadherin, and Zeb1 (Figures 6C and 6D), phenocopying the effects we observed with TAZ KD in leader cells.

Leader cells treated with TAK-981 exhibited reduced migration (Figure S9D). Additionally, TAK-981 reduced the invasive potential and proliferation of leader and follower cells and their mixes in 3D cultures (Figures 6E and 6F). To further demonstrate that the effects of TAK-981 were mediated via suppression of YAP and TAZ, we tested the effect of TAK-981 treatment on TAZ-overexpressing leader cells mixed with follower cells in a spheroid invasion assay. TAZ overexpression in leader cells restored both pAKT expression and the invasion

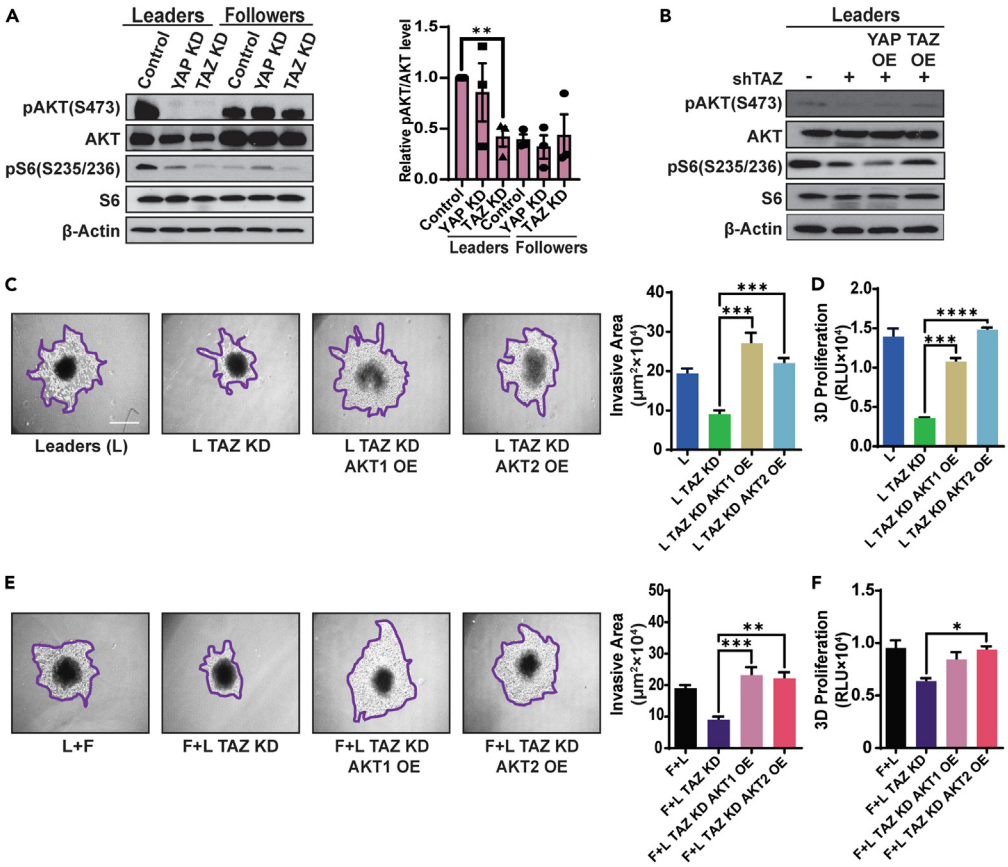

Figure 4. TAZ-regulated collective invasion is rescued by AKT OE

(A and B) Whole cell lysate of leader and follower non-targeting (control) or YAP/TAZ shRNA KD cells (cells from Figure 1D) or leader TAZ-KD cells OE YAP or TAZ evaluated for expression of indicated proteins using β-actin as a loading control. Representative blots from one of three independent experiments presented. pAKT/AKT quantification data represented mean ± SEM from three independent experiments.

(C–F) Invasion and proliferation evaluated (C and D) in spheroids generated from leader cells or TAZ-KD leader cells OE AKT1 or AKT2, or (E and F) in mixes with follower cells (1:9 ratio) with corresponding quantification of invasive area. ($n = 4$; scale bar, 100 μm). Data are represented as mean ± SEM. An ordinary one-way ANOVA with a Tukey's multiple comparisons test was used to determine significance compared to control or as indicated. *$p < 0.05$ **$p < 0.01$, ***$p < 0.001$, ****$p < 0.0001$ compared to the indicated group.

of leader cell spheroids treated with TAK-981 (Figure S12). TAZ overexpression promoted resistance to TAK-981, suggesting TAK-981 reduction of TAZ is required to prevent invasion (Figure S12).

We also assessed the effect of TAK-981 on proliferation of leaders, followers, and other parental lung cancer cell lines. TAK-981 significantly decreased the proliferation of leader cells and lung cancer cells in a dose-dependent manner, with no effect on the proliferation of followers (Figures S9A and S9B). In sum, our model outlines how YAP and TAZ intra-tumoral heterogeneity regulates collective invasion that is inhibited by SUMOylation inhibitor TAK-981. Higher TAZ in leader cells supports invasion via EGFR-AKT signaling, and active AKT blocks GSK3β to prevent TAZ from being degraded by βTrCP (Figure 6G).

SUMOylation inhibitor TAK-981 suppresses tumor growth *in vivo*

Our findings show that TAK-981 effectively targets the collective invasion of leader and follower cells. To investigate the efficacy of TAK-981 in other heterogeneous lung cancer parental cell lines, TAK-981 was administered in a panel of NSCLC cell lines with different KRAS/EGFR/STK11/P53 mutational profiles. TAK-981 treatment markedly reduced the proliferation of these cell lines and YAP, TAZ, and pAKT/AKT expression (Figures 7A and S5B). Furthermore, 3D collective invasion of a panel of NSCLC lines was significantly inhibited by TAK-981 (Figure 7B). To evaluate the efficacy of TAK-981 *in vivo*, H1299 cells were injected subcutaneously into non-obese diabetic severe combined immunodeficiency gamma (NSG) mice following the scheme outlined in Figure 7C. When tumors were palpable (3 weeks after injection), mice were treated with TAK-981 (25 mg/kg) or vehicle control intraperitoneally thrice weekly and tumor growth and animal body weight monitored till sacrifice on day 45. TAK-981-treated mice showed a significant reduction in tumor growth compared with vehicle-treated mice determined by endpoint tumor weight evaluation (Figure 7D). Additionally, TAK-981-treated mice exhibited significant reduction in tumor volume

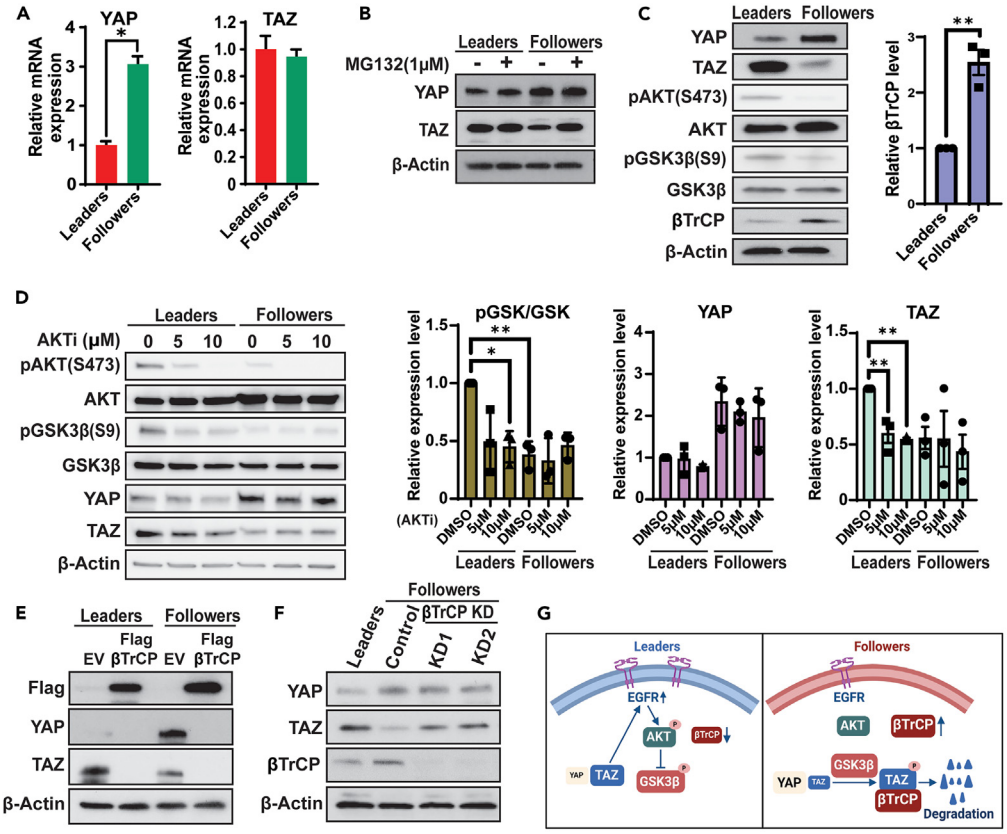

Figure 5. AKT-GS3β-βTrCP axis contributes to differential TAZ expression in follower and leader cells

(A) Evaluation of YAP and TAZ mRNA expression in leader and follower cells.

(B) YAP, TAZ, and β-actin expression in leader and follower cells treated with indicated doses of MG132 for 16 h.

(C) Whole cell lysates of leader and follower cells analyzed for βTrCP, AKT, GSK3β, and their phosphorylation status using β-actin as a loading control. βTrCP expression levels were quantified, and data represent mean ± SEM from $n = 3$.

(D) Indicated proteins evaluated and quantified in leader and follower cells treated with indicated doses of AKTi for 24 h. Data represent mean ± SEM from $n = 3$.

(E) Whole cell lysates of leader and follower cells expressing non-targeting control or βTrCP-directed shRNA evaluated for the indicated proteins.

(F) Evaluation of indicated proteins in leader and follower cells overexpressing βTrCP. Representative blot from one of three independent experiments presented.

(G) Schematic showing the mechanistic basis for differential expression of TAZ in leader and follower cells, created with Biorender.com. Data are represented as mean ± SEM. An ordinary one-way ANOVA with a Tukey's multiple comparisons test or t test was used to determine significance compared to control or as indicated. *$p < 0.05$ **$p < 0.01$ compared to the indicated group in the *post hoc* tests.

compared to the vehicle-treated animals (Figures 7D–7F). TAK-981 was well tolerated during treatment, supported by a gain in average body weight (Figure S13). TAK-981-treated tumors exhibited downregulated YAP, TAZ, CTGF, and N-cadherin expression and variable decrease in pAKT/AKT expression (Figure 7G). Lastly, examination of lung and liver histology demonstrated a significant reduction of micro and macro metastases (Figures 7H and 7I). Livers of treated animals showed fibrin around the capsule and extramedullary hematopoiesis (EMH) of indeterminate significance. In sum, TAK-981 inhibits YAP/TAZ-driven signaling and tumor growth in a preclinical murine model of NSCLC.

DISCUSSION

Intra-tumoral phenotypic heterogeneity sustains cooperative biology, underpinning several hallmark characteristics of cancer.[12] Combination therapies thus need to be designed to target distinct phenotypes that cooperate to drive cancer development, progression, and therapy resistance. A large focus in cancer therapy has been to investigate and target the most represented genetic/epigenetic drivers and key signaling pathway effectors with less focus on strategies to co-target distinct cooperative phenotypes such as proliferative and invasive cells, quiescent and cycling cells, drug-resistant persister cells, and their sensitive counterparts. These observations underscore the importance of identifying phenotypic heterogeneity and their drivers.

Alterations in the extrinsic stroma and microenvironment are considered causal in cancer metastases and pathogenesis.[44] The transcriptional co-activators YAP and TAZ are at the nexus of integrating mechanical stress and environmental cues to intracellular biology regulating survival,

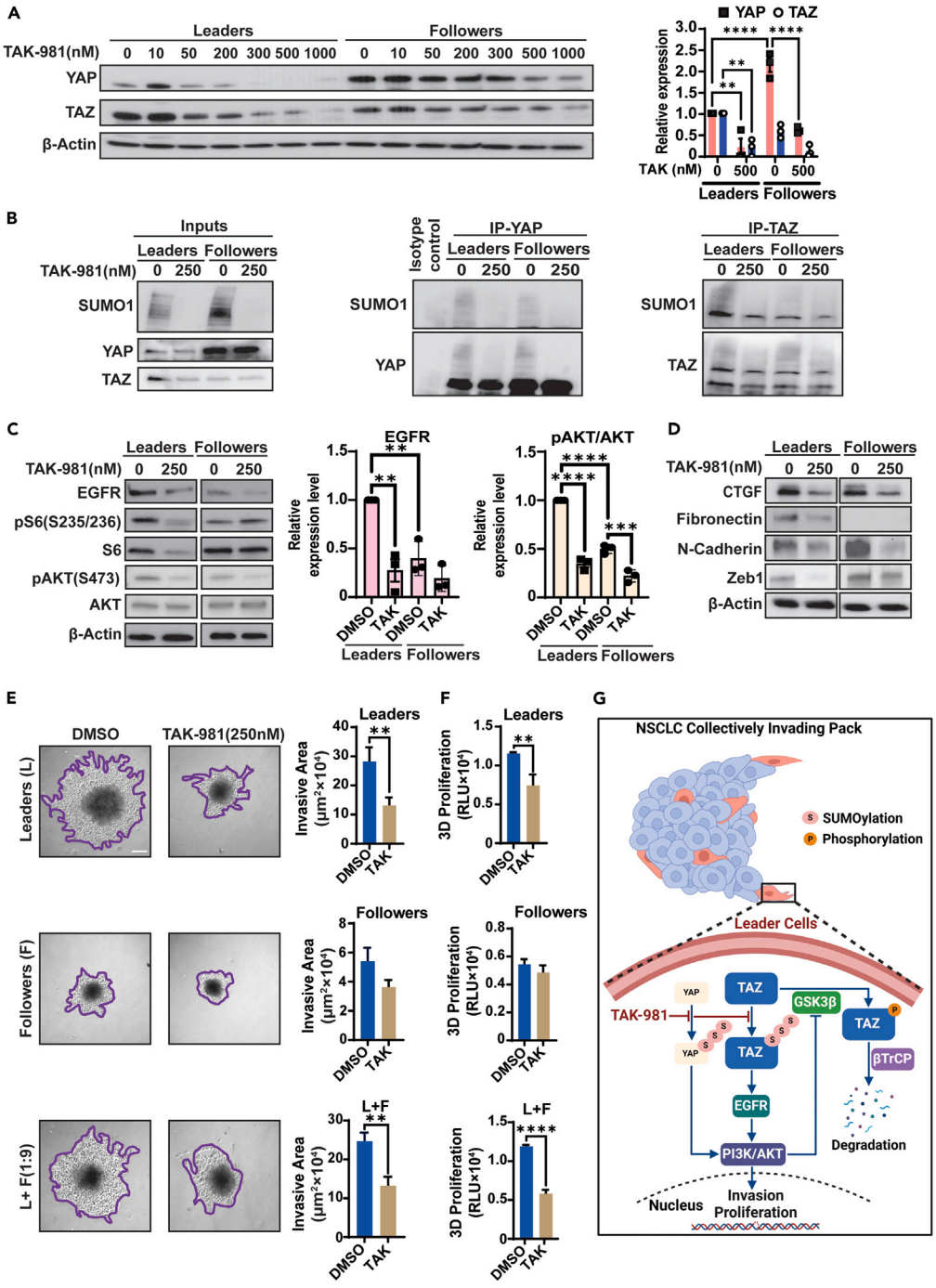

Figure 6. SUMOylation inhibitor TAK-981 suppresses YAP and TAZ SUMOylation and YAP/TAZ expression

(A) Leader and follower cells treated with indicated doses of TAK-981 for 72 h were evaluated for YAP and TAZ. Expression levels normalized to β-actin (loading control) are presented. Data are presented as means ± SEM from three independent repeats. One representative experiment of an $n = 3$ is shown.

(B) Immunoprecipitates of YAP and TAZ from whole cell lysates leader and follower cells treated +/− TAK-981 for 6 h were evaluated for SUMO-1.

(C and D) Leader and follower cells treated with TAK-981 for 24 h followed by analysis of whole cell lysates for indicated proteins. Quantification of indicated protein represented as mean ± SEM from three independent repeats.

(E and F) Spheroids generated with leader cells, follower cells, or mixes of 90% follower cells and 10% leader cells (L:F, 1:9) treated with either DMSO or indicated doses of TAK-981 were evaluated for invasive area with quantification of invasive area ($n = 4$; scale bar, 100 μm).

Figure 6. *Continued*

(G) Schematic depiction of YAP- and TAZ-driven regulation of intra-tumoral heterogeneity supporting collective invasion that is inhibited by TAK-981, created with Biorender.com. Data are represented as mean ± SEM. An ordinary one-way ANOVA with a Tukey's multiple comparisons test or t test was used to determine significance compared to control or as indicated. $^{**}p < 0.01$, $^{***}p < 0.001$, $^{****}p < 0.0001$ compared to the indicated group in the *post hoc* tests.

growth, and invasion.[45] YAP and TAZ are critical during development, and their activities are largely suppressed in adult tissues, except for roles in tissue repair, negating their requirement for normal adult functions.[46] Importantly, these transcription factors are re-expressed in cancer cells to regulate diverse sets of biological processes, providing a strong rationale for therapeutic targeting. What distinguishes these transcription factors from other drivers of oncogenesis is that their functional roles are not generally consequent to proximal mutations/amplifications. YAP and TAZ are responsive to extrinsic cues such as mechanical stress, 3D architecture, the extracellular matrix (ECM), and inflammation, in contrast to growth factor/cytokine-driven oncogenic pathways. YAP and TAZ shuttle between the nucleus and cytoplasm and co-activate transcription of genes largely in association with the TEAD family members.[46,47] Despite 57% sequence similarity,[29] RNA-seq of H1299 NSCLC cells exhibiting suppression of YAP or TAZ shows regulation of both redundant and, importantly, non-overlapping genes.[29] YAP-regulated genes were connected to proliferation and cell cycle while TAZ-regulated genes were connected to EMT and invasion and migration. It is thus not surprising that the original gene identified in *Drosophila* (Yorkie) has evolved to two orthologs regulating redundant but importantly unique repertoires of genes. TAZ expression was found to increase with cancer progression with higher expression detected in stage IV lung adenocarcinomas.[30,48,49] TAZ is recognized as an oncogene in NSCLC[50] with several oncogenic roles such as facilitating transforming growth factor β β1 EMT in oral squamous cell carcinoma[51] and in Src-driven metastases in breast cancer and melanoma.[52]

Our study importantly demonstrates an intra-tumoral division of labor driven by YAP and TAZ. We identify higher expression of TAZ in leader invasive cells in contrast to elevated expression of YAP in the proliferative follower cells of collectively invading NSCLC, correlating with elevated nuclear expression. While these observations stem from one follower/leader pair isolated from the H1299 line, the need to target both YAP and TAZ was validated across a broader panel of lines. We also detected similar heterogeneity in YAP and TAZ NSCLC patients' specimens by immunohistochemistry (IHC) and found that fibronectin expression (expressed at higher levels in our leader cells) correlates with TAZ, not YAP, expression in NSCLC patients. We showed through suppression of YAP or TAZ their necessity in supporting the proliferative vs. invasive phenotypes of follower and leader cells, respectively, and importantly their collective invasion. Mechanical stress and ECM rigidity can drive nuclear localization of YAP/TAZ, EMT, and the migratory phenotype fueling metastases.[53] Interestingly, in collectively invading breast cancer cells, collagen-induced YAP increases leader cell emergence[54] underscoring how YAP or TAZ are differentially engaged to promote collective invasion. The cytoskeletal remodeling fueling migration is reported to consume 50% of the cellular ATP budget,[55,56] concordant with our observation that invasive leader cells are reliant on OXPHOS to sustain their migratory phenotype.[20] In line with these observations, we found TAZ suppression in leader cells to reduce oxygen consumption, OXPHOS, and migration/invasion.

EMT is known to promote invasion and metastases. In this process, epithelial cells lose polarity and intercellular cohesion to adopt a mesenchymal, fibroblast-like, migratory phenotype. EMT is marked by elevated expression of cell adhesion molecules such as N-cadherin, Zeb1, fibronectin, and CTGF, a known TAZ target gene.[57–60] Importantly, suppression of TAZ, in contrast to YAP, in leader cells reduces expression of N-cadherin, fibronectin, CTGF, and Zeb1, concordant with inhibition of migratory/invasive potential. YAP suppression reduced the expression of CTGF and pAKT, supportive of YAP's contribution to invasive signaling. Our results thus further shed light on how TAZ mechanistically contributes to the invasiveness of leader like cells.

In sum, our results strongly support the utility of targeting both TAZ- and YAP-driven effects to comprehensively target NSCLC. Targeting transcription factors, however, can be challenging. Current strategies targeting proteins include inhibiting transcription factor-coactivator protein-protein or protein-DNA interactions, altering the transcription factor expression level by altering post-translational modifications such as ubiquitinylation or SUMOylation that regulate stability and proteasomal degradation, or direct targeting of the protein using proteolysis targeting chimaeras.[61] The small-molecule benzoporphyrin VP (Visudyne), identified by Liu-Chittenden,[62] disrupts the YAP-TEAD interaction in the absence of photo-activation, blocking YAP-driven oncogenic growth. VP has historically been used as a photosensitizer in photodynamic therapy for the treatment of subfoveal choroidal neovascularization.[40] VP has shown anticancer effects against several solid tumors including breast, prostate, pancreatic, and esophageal cancer when combined with conventional chemotherapy.[41,62,63] We found that VP treatment did not impact TAZ expression in leader cells; however, it significantly reduced YAP and TAZ expression in follower cells. Additionally, VP did not impact the migratory and invasive potential of leader cells, supporting our premise to investigate other methods to co-target both YAP and TAZ expression. TEAD inhibitors, currently in clinical trials, target the autopalmitoylation of TEADs disrupting their interaction with YAP/TAZ. While this strategy targets YAP/TAZ/TEAD-driven gene expression, the efficacy and off-target toxicities are yet to be determined.[64]

Our evaluation of transcript expression shows elevated YAP mRNA in follower vs. leader cells, but comparable TAZ mRNA expression. This suggests that elevated TAZ protein expression in leader over follower cells is likely consequent to post-transcriptional/translational mechanisms. Phosphorylation, ubiquitination, acetylation, methylation, SUMOylation, and O-GlcNAcylation play a central role in regulating YAP/TAZ stability.[65–69] The E3 Ub ligase (βTrCP) is well documented to regulate TAZ expression. YAP and TAZ are ubiquitinated by F box protein βTrCP in response to LATS-mediated phosphorylation of YAP and TAZ within their phosphodegron (DSGxS sequence).[38,70] Additionally, GSK3 can phosphorylate the N-terminal phosphodegron in TAZ. The $SCF^{\beta TrCP}$ E3 Ub ligase complex binds phosphorylated TAZ leading to its ubiquitylation and degradation.[38] We showed elevated AKT phosphorylation in leader cells that likely contributes to GSK3β inhibition preventing TAZ phosphorylation and βTrCP-mediated degradation. Correspondingly we found elevated expression of βTrCP in follower vs. leader cells, inversely correlating with TAZ expression. Our inquiry of follower leader RNA-seq showed several E3 Ub ligases such as MARCH4,

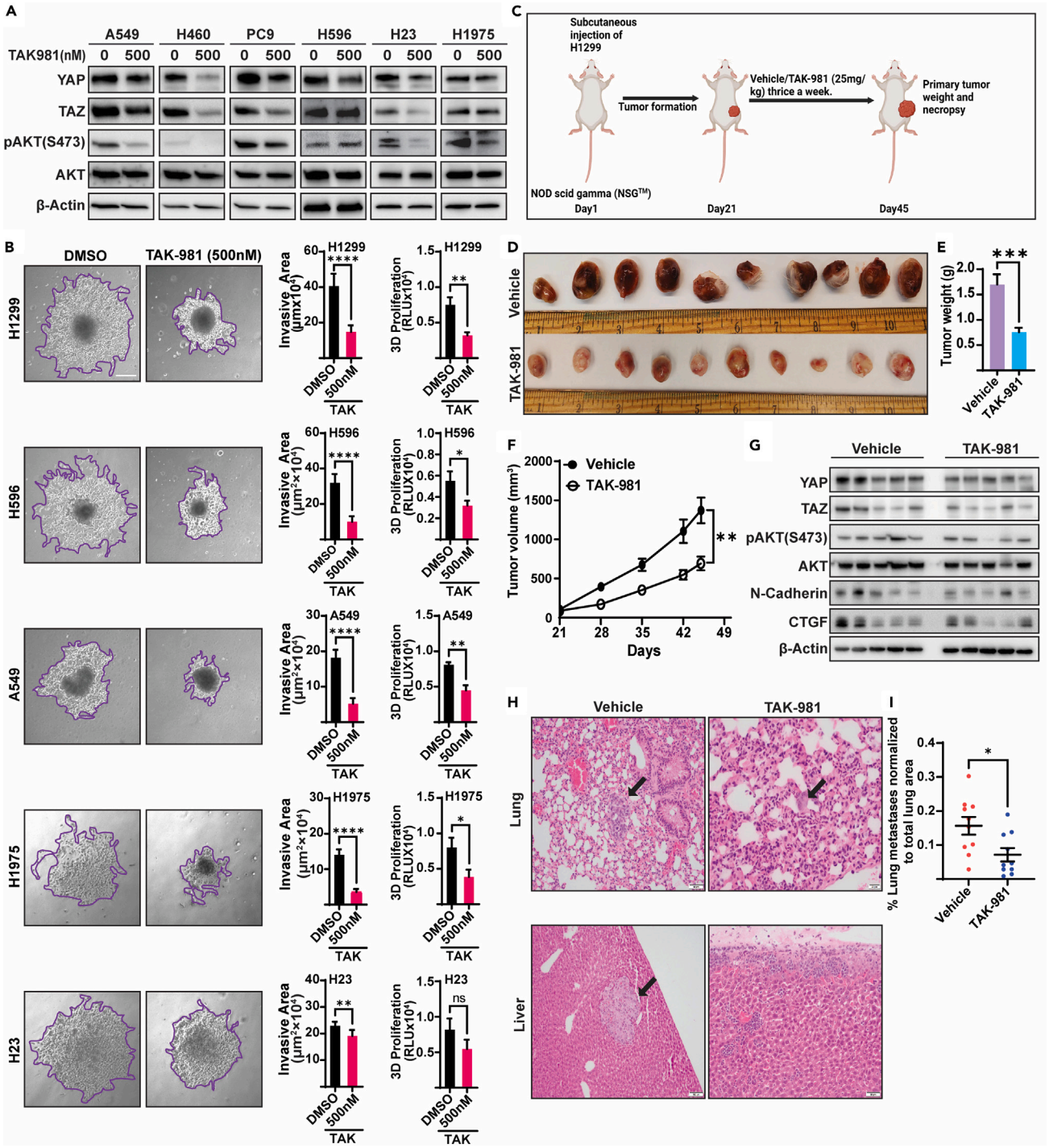

Figure 7. TAK-981 inhibits the *in vitro* proliferation and collective invasion of NSCLC lines and *in vivo* tumor growth and metastases in a preclinical model of NSCLC

(A) Indicated proteins and β-actin (loading control) were assessed in A549, H460, PC9, H596, H23, and H1975 cells after 72 h of TAK-981 treatment.

(B) Spheroids generated with indicated cell lines treated with either DMSO or TAK-981 (500 nM) were evaluated for invasive area and proliferation with quantification of invasive area (n = 5; scale bar, 100 μm).

(C) Experimental treatment strategy used in H1299-NSG murine tumor model. Tumors were subcutaneously injected in NSG mice (n = 10 mice per group) and randomized to two groups when tumors were palpable (approximately three weeks). Mice were treated with vehicle or 25 mg/kg TAK-981 thrice weekly.

(D) Bright-field images of tumors isolated from vehicle- and TAK-981-treated mice.

Figure 7. *Continued*

(E and F) (E) Mean tumor weight and (F) mean tumor volume of mice treated with vehicle or TAK-981.

(G) Western blot to assess expression level of indicated proteins in tumors from vehicle- and TAK-981-treated mice.

(H) Representative images of lung and liver macro mets (indicated by arrows) identified from vehicle-treated groups. TAK-981-treated lung indicates (with arrow) a micro met while a liver section shows EMH and fibrin overlaying the capsule.

(I) Percentage lung metastases was calculated by quantification of total macro and micro mets area normalized to total area in H&E-stained lung sections from vehicle- and TAK-981-treated mice ($n = 10$). Data are represented as mean ± SEM. t test was used to determine significance compared to control or as indicated. *$p < 0.05$, **$p < 0.01$, ***$p < 0.001$, ****$p < 0.0001$ compared to the indicated group in the *post hoc* tests.

SMURF2, and TRIM3 to be increased in follower cells. Suppression of these E3 Ub ligases restored TAZ expression in follower cells. Among the investigated E3 UB ligases, βTrCP was most effective in rescuing TAZ protein from degradation, which was further confirmed by βTrCP KD and overexpression.

SUMOylation plays a pivotal role in regulating YAP and TAZ stability by antagonizing ubiquitination. SUMOylation is a reversible post-translational modification involving covalent attachment of a SUMO protein to lysine residues of target proteins.[42] While ubiquitination is primarily involved in protein degradation, SUMOylation plays a broader role in various cellular processes involved in cell growth and survival. Hence, the balance between SUMOylation and deSUMOylation is crucial in maintaining cellular integrity.[42]

Because enzymes in the SUMOylation pathway are upregulated and associated with poor prognosis in several cancers, there is increased interest in the development of SUMOylation inhibitors. ML-792 is a synthetic selective small-molecule inhibitor of SUMO-activating enzyme subunit (SAE2) inhibiting SUMOylation.[71,72] Subasumstat (TAK-981) is derived from ML-792. TAK-981 shows enhanced selectivity and durability of the SUMO-inhibitor adduct and was shown to inhibit tumor growth at lower concentrations than ML-792.[71] Our findings corroborate the previously identified SUMOylation of YAP[73] and reports SUMOylation of TAZ. Interestingly, we detected increased TAZ SUMOylation in leader cells; hence, inhibiting SUMOylation would be an attractive strategy to target YAP and TAZ stability in leader cells. SUMOylation was overall elevated in leader cells, and treatment with TAK-981 reduced SUMOylation of both YAP and TAZ and their expression. This is a previously unreported documentation of TAK-981 to reduce both YAP and TAZ expression. Importantly, our preclinical evaluation of TAK-981 in H1299 cells introduced into NSG mice showed a reduction of tumor burden and micro and macro metastases. TAK-981 was found to reduce both YAP and TAZ expression in tumors, corroborating our *in vitro* findings detected across several NSCLC lines expressing common driver genetic lesions.

EGFR activity indirectly inactivates LATS1/2, leading to increased nuclear localization of YAP in head and neck squamous cell carcinoma.[74] YAP/TAZ increases expression of EGFR ligands such as amphiregulin (AREG) to increase EGFR signaling.[75,76] EGFR is also a YAP/TEAD target,[74] and increased YAP and TAZ expression has been observed in EGFR mutant NSCLC.[77] Our studies demonstrate elevated expression of EGFR in invasive leader cells in contrast to the proliferative follower cells. Additionally, EGFR expression in leader cells was regulated by TAZ but not YAP, identifying the unique consequences of differential YAP and TAZ expression. The EGFR-TAZ connection was further corroborated by elevated AKT activity, a well-known downstream effector of EGFR, in invasive leader cells and downregulation of AKT upon TAZ suppression.[37] We interestingly detected reduction of pAKT in YAP-KD leader cells despite maintenance of EGFR expression, suggesting an additional EGFR-independent path to regulating AKT phosphorylation. The effects of TAZ and EGFR suppression on leader cell invasion were reversed by AKT overexpression, supporting the downstream role of AKT in TAZ-regulated invasion. In contrast, overexpression of YAP in TAZ-KD leaders rescued AKT with minimal rescue of EGFR expression, supportive of the role of TAZ in regulating EGFR expression.

Collectively, our studies reveal how invasive and proliferative phenotypes in NSCLC are maintained by heterogeneous YAP and TAZ expression. We provide rationale for a translationally relevant strategy that can be leveraged to target both YAP and TAZ proteins centered on the use of the newly developed SUMOylation inhibitor, TAK-981. Our observations importantly underscore the continued need to identify and target phenotypic heterogeneity that supports collective cell invasion in NSCLC.

Limitations of the study

The limitations of our study include lack of defined leader and follower cell markers restricting inquiry in collectively invading human NSCLC. Additionally, there is a lack of preclinical NSCLC models that can effectively isolate the effects of perturbing leader vs. follower cells in metastasis. Furthermore, while the study demonstrates the efficacy of TAK-981 in suppressing YAP and TAZ in a preclinical murine model, further validation in human NSCLC metastases is warranted.

RESOURCE AVAILABILITY

Lead contact

Further information, resources, and reagents requests should be directed to and will be fulfilled by the lead contact, Mala Shanmugam (mala.shan@emory.edu).

Materials availability

All reagents generated during this study are available from the lead contact.

Data and code availability

- All data reported in this paper will be shared by the lead contact upon request.
- This paper does not report original code.
- Any additional information required to reanalyze the data reported in this paper is available from the lead contact upon request.

- Access to molecular profiling source data is controlled and managed by the Winship Cancer Institute of Emory University and is not publicly available, per the Data Use Agreement signed by the investigators of this research. Summary level data may be provided upon request.

ACKNOWLEDGMENTS

We would like to thank Ms Tala O Khatib, BS, Marcus Lab, for her assistance with providing NSCLC cell lines and Dr Anthea Hammond, Emory University, for editorial assistance. Research reported in this publication was funded by NCI/NIH R01 CA247367-01A1 awarded to M.S. and A.I.M., and in part by the Integrated Cellular Imaging Core and Winship Flow Cytometry Core shared resources of Winship Cancer Institute of Emory University; Developmental Funds from the Winship Cancer Institute of Emory University; and the NIH/NCI P30CA138292 award and NIH NCI R50CA265345 to J.K.M.

AUTHOR CONTRIBUTIONS

Conceptualization, R.S. and M.S.; methodology, R.S., S.S., P.S., L.M., J.K.M., and V.Y.M.; bioinformatic analysis of TCGA and Winship cBioPortal dataset, P.S., G.J., and M.B.; mouse studies, R.S., P.S., J.K., J.K.M., M.A.R., and C.H.; manuscript writing, M.S. and R.S.; manuscript review and editing, R.S., A.H.V., S.S., L.M., A.I.M., T.L., M.G.-R., S.-Y.S., and M.S.

DECLARATION OF INTERESTS

T.L. is on the advisory board for Mirati, AstraZeneca, Merck, Takeda, EMD Serono, Eisai, and Jazz; is a consultant for Merck, Daiichi-Sankyo, Janssen, Eisai, Novocure, Amgen, Roche, Regeneron, and Catalyst; and has research funding to institution from Pfizer, Advaxis, and Bayer.

STAR★METHODS

Detailed methods are provided in the online version of this paper and include the following:

- KEY RESOURCES TABLE
- EXPERIMENTAL MODEL AND STUDY PARTICIPANT DETAILS
  - *In vivo* animal studies
  - Cell lines
  - Cell culture
- METHOD DETAILS
  - Generation of shRNA KDs
  - Reverse transcription quantitative polymerase chain reaction
  - Immunoblotting
  - Cell viability/proliferation assays
  - Live cell oxygen consumption and extracellular acidification rates
  - Spheroid formation and invasion assays
  - Scratch assay
  - *In vivo* mouse studies
  - Immunohistochemistry (IHC) staining
  - Immunofluorescence and confocal microscopy
  - Coimmunoprecipitation
  - Bioinformatics analysis
- QUANTIFICATION AND STATISTICAL ANALYSIS

SUPPLEMENTAL INFORMATION

Supplemental information can be found online at https://doi.org/10.1016/j.isci.2024.111133.

Received: February 29, 2024
Revised: June 15, 2024
Accepted: October 7, 2024
Published: October 11, 2024

REFERENCES

1. Sung, H., Ferlay, J., Siegel, R.L., Laversanne, M., Soerjomataram, I., Jemal, A., and Bray, F. (2021). Global Cancer Statistics 2020: GLOBOCAN Estimates of Incidence and Mortality Worldwide for 36 Cancers in 185 Countries. CA A Cancer J. Clin. *71*, 209–249. https://doi.org/10.3322/caac.21660.
2. Torre, L.A., Bray, F., Siegel, R.L., Ferlay, J., Lortet-Tieulent, J., and Jemal, A. (2015). Global cancer statistics, 2012. CA A Cancer J. Clin. *65*, 87–108. https://doi.org/10.3322/caac.21262.
3. Xu, Z., Yang, Q., Chen, X., Zheng, L., Zhang, L., Yu, Y., Chen, M., You, Q., and Sun, J. (2019). Clinical associations and prognostic value of site-specific metastases in non-small cell lung cancer: A population-based study. Oncol. Lett. *17*, 5590–5600. https://doi.org/10.3892/ol.2019.10225.
4. Tamura, T., Kurishima, K., Nakazawa, K., Kagohashi, K., Ishikawa, H., Satoh, H., and Hizawa, N. (2015). Specific organ metastases and survival in metastatic non-small-cell lung cancer. Mol. Clin. Oncol. *3*, 217–221. https://doi.org/10.3892/mco.2014.410.
5. Siegel, R.L., Miller, K.D., and Jemal, A. (2020). Cancer statistics, 2020. CA A Cancer J. Clin. *70*, 7–30. https://doi.org/10.3322/caac.21590.
6. Friedl, P., and Gilmour, D. (2009). Collective cell migration in morphogenesis, regeneration and cancer. Nat. Rev. Mol. Cell Biol. *10*, 445–457. https://doi.org/10.1038/nrm2720.
7. Konen, J., Summerbell, E., Dwivedi, B., Galior, K., Hou, Y., Rusnak, L., Chen, A., Saltz, J., Zhou, W., Boise, L.H., et al. (2017). Image-guided genomics of phenotypically heterogeneous populations reveals vascular signalling during symbiotic collective cancer invasion. Nat. Commun. *8*, 15078. https://doi.org/10.1038/ncomms15078.
8. Cheung, K.J., Gabrielson, E., Werb, Z., and Ewald, A.J. (2013). Collective invasion in breast cancer requires a conserved basal epithelial program. Cell *155*, 1639–1651. https://doi.org/10.1016/j.cell.2013.11.029.
9. Westcott, J.M., Prechtl, A.M., Maine, E.A., Dang, T.T., Esparza, M.A., Sun, H., Zhou, Y., Xie, Y., and Pearson, G.W. (2015). An epigenetically distinct breast cancer cell

subpopulation promotes collective invasion. J. Clin. Invest. *125*, 1927–1943. https://doi.org/10.1172/JCI77767.

10. Morris, L.G.T., Riaz, N., Desrichard, A., Şenbabaoğlu, Y., Hakimi, A.A., Makarov, V., Reis-Filho, J.S., and Chan, T.A. (2016). Pan-cancer analysis of intratumor heterogeneity as a prognostic determinant of survival. Oncotarget *7*, 10051–10063. https://doi.org/10.18632/oncotarget.7067.
11. McGranahan, N., and Swanton, C. (2015). Biological and therapeutic impact of intratumor heterogeneity in cancer evolution. Cancer Cell *27*, 15–26. https://doi.org/10.1016/j.ccell.2014.12.001.
12. Sottoriva, A., Spiteri, I., Piccirillo, S.G.M., Touloumis, A., Collins, V.P., Marioni, J.C., Curtis, C., Watts, C., and Tavaré, S. (2013). Intratumor heterogeneity in human glioblastoma reflects cancer evolutionary dynamics. Proc. Natl. Acad. Sci. USA *110*, 4009–4014. https://doi.org/10.1073/pnas.1219747110.
13. Brocks, D., Assenov, Y., Minner, S., Bogatyrova, O., Simon, R., Koop, C., Oakes, C., Zucknick, M., Lipka, D.B., Weischenfeldt, J., et al. (2014). Intratumor DNA methylation heterogeneity reflects clonal evolution in aggressive prostate cancer. Cell Rep. *8*, 798–806. https://doi.org/10.1016/j.celrep.2014.06.053.
14. Cheung, K.J., Padmanaban, V., Silvestri, V., Schipper, K., Cohen, J.D., Fairchild, A.N., Gorin, M.A., Verdone, J.E., Pienta, K.J., Bader, J.S., and Ewald, A.J. (2016). Polyclonal breast cancer metastases arise from collective dissemination of keratin 14-expressing tumor cell clusters. Proc. Natl. Acad. Sci. USA *113*, E854–E863. https://doi.org/10.1073/pnas.1508541113.
15. Haney, S., Konen, J., Marcus, A.I., and Bazhenov, M. (2018). The complex ecosystem in non small cell lung cancer invasion. PLoS Comput. Biol. *14*, e1006131. https://doi.org/10.1371/journal.pcbi.1006131.
16. Khalil, A.A., and Friedl, P. (2010). Determinants of leader cells in collective cell migration. Integr. Biol. *2*, 568–574. https://doi.org/10.1039/c0ib00052c.
17. Moffitt, L., Karimnia, N., Stephens, A., and Bilandzic, M. (2019). Therapeutic Targeting of Collective Invasion in Ovarian Cancer. Int. J. Mol. Sci. *20*, 1466. https://doi.org/10.3390/ijms20061466.
18. Mayor, R., and Etienne-Manneville, S. (2016). The front and rear of collective cell migration. Nat. Rev. Mol. Cell Biol. *17*, 97–109. https://doi.org/10.1038/nrm.2015.14.
19. Summerbell, E.R., Mouw, J.K., Bell, J.S.K., Knippler, C.M., Pedro, B., Arnst, J.L., Khatib, T.O., Commander, R., Barwick, B.G., Konen, J., et al. (2020). Epigenetically heterogeneous tumor cells direct collective invasion through filopodia-driven fibronectin micropatterning. Sci. Adv. *6*, eaaz6197. https://doi.org/10.1126/sciadv.aaz6197.
20. Commander, R., Wei, C., Sharma, A., Mouw, J.K., Burton, L.J., Summerbell, E., Mahboubi, D., Peterson, R.J., Konen, J., Zhou, W., et al. (2020). Subpopulation targeting of pyruvate dehydrogenase and GLUT1 decouples metabolic heterogeneity during collective cancer cell invasion. Nat. Commun. *11*, 1533. https://doi.org/10.1038/s41467-020-15219-7.
21. Pan, D. (2010). The hippo signaling pathway in development and cancer. Dev. Cell *19*, 491–505. https://doi.org/10.1016/j.devcel.2010.09.011.
22. Zhao, B., Li, L., Lei, Q., and Guan, K.L. (2010). The Hippo-YAP pathway in organ size control and tumorigenesis: an updated version. Genes Dev. *24*, 862–874. https://doi.org/10.1101/gad.1909210.
23. Halder, G., and Johnson, R.L. (2011). Hippo signaling: growth control and beyond. Development *138*, 9–22. https://doi.org/10.1242/dev.045500.
24. Zhang, W., Gao, Y., Li, F., Tong, X., Ren, Y., Han, X., Yao, S., Long, F., Yang, Z., Fan, H., et al. (2015). YAP promotes malignant progression of Lkb1-deficient lung adenocarcinoma through downstream regulation of survivin. Cancer Res. *75*, 4450–4457. https://doi.org/10.1158/0008-5472.CAN-14-3396.
25. Zhang, X., Yang, L., Szeto, P., Abali, G.K., Zhang, Y., Kulkarni, A., Amarasinghe, K., Li, J., Vergara, I.A., Molania, R., et al. (2020). The Hippo pathway oncoprotein YAP promotes melanoma cell invasion and spontaneous metastasis. Oncogene *39*, 5267–5281. https://doi.org/10.1038/s41388-020-1362-9.
26. Yu, B., Su, J., Shi, Q., Liu, Q., Ma, J., Ru, G., Zhang, L., Zhang, J., Hu, X., and Tang, J. (2022). KMT5A-methylated SNIP1 promotes triple-negative breast cancer metastasis by activating YAP signaling. Nat. Commun. *13*, 2192. https://doi.org/10.1038/s41467-022-29899-w.
27. Lei, Q.Y., Zhang, H., Zhao, B., Zha, Z.Y., Bai, F., Pei, X.H., Zhao, S., Xiong, Y., and Guan, K.L. (2008). TAZ promotes cell proliferation and epithelial-mesenchymal transition and is inhibited by the hippo pathway. Mol. Cell Biol. *28*, 2426–2436. https://doi.org/10.1128/MCB.01874-07.
28. Zhang, H., Liu, C.Y., Zha, Z.Y., Zhao, B., Yao, J., Zhao, S., Xiong, Y., Lei, Q.Y., and Guan, K.L. (2009). TEAD transcription factors mediate the function of TAZ in cell growth and epithelial-mesenchymal transition. J. Biol. Chem. *284*, 13355–13362. https://doi.org/10.1074/jbc.M900843200.
29. Shreberk-Shaked, M., Dassa, B., Sinha, S., Di Agostino, S., Azuri, I., Mukherjee, S., Aylon, Y., Blandino, G., Ruppin, E., and Oren, M. (2020). A Division of Labor between YAP and TAZ in Non-Small Cell Lung Cancer. Cancer Res. *80*, 4145–4157. https://doi.org/10.1158/0008-5472.CAN-20-0125.
30. Lau, A.N., Curtis, S.J., Fillmore, C.M., Rowbotham, S.P., Mohseni, M., Wagner, D.E., Beede, A.M., Montoro, D.T., Sinkevicius, K.W., Walton, Z.E., et al. (2014). Tumor-propagating cells and Yap/Taz activity contribute to lung tumor progression and metastasis. EMBO J. *33*, 468–481. https://doi.org/10.1002/embj.201386082.
31. Lintz, M., Muñoz, A., and Reinhart-King, C.A. (2017). The Mechanics of Single Cell and Collective Migration of Tumor Cells. J. Biomech. Eng. *139*, 210051–210059. https://doi.org/10.1115/1.4035121.
32. Bethune, G., Bethune, D., Ridgway, N., and Xu, Z. (2010). Epidermal growth factor receptor (EGFR) in lung cancer: an overview and update. J. Thorac. Dis. *2*, 48–51.
33. Ando, T., Arang, N., Wang, Z., Costea, D.E., Feng, X., Goto, Y., Izumi, H., Gilardi, M., Ando, K., and Gutkind, J.S. (2021). EGFR Regulates the Hippo pathway by promoting the tyrosine phosphorylation of MOB1. Commun. Biol. *4*, 1237. https://doi.org/10.1038/s42003-021-02744-4.
34. Gao, M., Fu, Y., Zhou, W., Gui, G., Lal, B., Li, Y., Xia, S., Ji, H., Eberhart, C.G., Laterra, J., and Ying, M. (2021). EGFR Activates a TAZ-Driven Oncogenic Program in Glioblastoma. Cancer Res. *81*, 3580–3592. https://doi.org/10.1158/0008-5472.Can-20-2773.
35. He, C., Mao, D., Hua, G., Lv, X., Chen, X., Angeletti, P.C., Dong, J., Remmenga, S.W., Rodabaugh, K.J., Zhou, J., et al. (2015). The Hippo/YAP pathway interacts with EGFR signaling and HPV oncoproteins to regulate cervical cancer progression. EMBO Mol. Med. *7*, 1426–1449. https://doi.org/10.15252/emmm.201404976.
36. Vigneswaran, K., Boyd, N.H., Oh, S.Y., Lallani, S., Boucher, A., Neill, S.G., Olson, J.J., and Read, R.D. (2021). YAP/TAZ Transcriptional Coactivators Create Therapeutic Vulnerability to Verteporfin in EGFR-mutant Glioblastoma. Clin. Cancer Res. *27*, 1553–1569. https://doi.org/10.1158/1078-0432.CCR-20-0018.
37. Sordella, R., Bell, D.W., Haber, D.A., and Settleman, J. (2004). Gefitinib-sensitizing EGFR mutations in lung cancer activate anti-apoptotic pathways. Science *305*, 1163–1167. https://doi.org/10.1126/science.1101637.
38. Huang, W., Lv, X., Liu, C., Zha, Z., Zhang, H., Jiang, Y., Xiong, Y., Lei, Q.Y., and Guan, K.L. (2012). The N-terminal phosphodegron targets TAZ/WWTR1 protein for SCFbeta-TrCP-dependent degradation in response to phosphatidylinositol 3-kinase inhibition. J. Biol. Chem. *287*, 26245–26253. https://doi.org/10.1074/jbc.M112.382036.
39. Cross, D.A., Alessi, D.R., Cohen, P., Andjelkovich, M., and Hemmings, B.A. (1995). Inhibition of glycogen synthase kinase-3 by insulin mediated by protein kinase B. Nature *378*, 785–789. https://doi.org/10.1038/378785a0.
40. Miller, J.W. (2008). Higher irradiance and photodynamic therapy for age-related macular degeneration (an AOS thesis). Trans. Am. Ophthalmol. Soc. *106*, 357–382.
41. Feng, J., Gou, J., Jia, J., Yi, T., Cui, T., and Li, Z. (2016). Verteporfin, a suppressor of YAP-TEAD complex, presents promising antitumor properties on ovarian cancer. OncoTargets Ther. *9*, 5371–5381. https://doi.org/10.2147/OTT.S109979.
42. Celen, A.B., and Sahin, U. (2020). Sumoylation on its 25th anniversary: mechanisms, pathology, and emerging concepts. FEBS J. *287*, 3110–3140. https://doi.org/10.1111/febs.15319.
43. Lapi, E., Di Agostino, S., Donzelli, S., Gal, H., Domany, E., Rechavi, G., Pandolfi, P.P., Givol, D., Strano, S., Lu, X., and Blandino, G. (2008). PML, YAP, and p73 are components of a proapoptotic autoregulatory feedback loop. Mol. Cell *32*, 803–814. https://doi.org/10.1016/j.molcel.2008.11.019.
44. Lu, P., Weaver, V.M., and Werb, Z. (2012). The extracellular matrix: a dynamic niche in cancer progression. J. Cell Biol. *196*, 395–406. https://doi.org/10.1083/jcb.201102147.
45. Halder, G., Dupont, S., and Piccolo, S. (2012). Transduction of mechanical and cytoskeletal cues by YAP and TAZ. Nat. Rev. Mol. Cell Biol. *13*, 591–600. https://doi.org/10.1038/nrm3416.
46. Zanconato, F., Cordenonsi, M., and Piccolo, S. (2016). YAP/TAZ at the Roots of Cancer. Cancer Cell *29*, 783–803. https://doi.org/10.1016/j.ccell.2016.05.005.
47. Chan, S.W., Lim, C.J., Loo, L.S., Chong, Y.F., Huang, C., and Hong, W. (2009). TEADs mediate nuclear retention of TAZ to promote oncogenic transformation. J. Biol. Chem. *284*, 14347–14358. https://doi.org/10.1074/jbc.M901568200.

48. Luo, J., Zou, H., Guo, Y., Tong, T., Chen, Y., Xiao, Y., Pan, Y., and Li, P. (2023). The oncogenic roles and clinical implications of YAP/TAZ in breast cancer. Br. J. Cancer *128*, 1611–1624. https://doi.org/10.1038/s41416-023-02182-5.
49. Xie, M., Zhang, L., He, C.S., Hou, J.H., Lin, S.X., Hu, Z.H., Xu, F., and Zhao, H.Y. (2012). Prognostic significance of TAZ expression in resected non-small cell lung cancer. J. Thorac. Oncol. *7*, 799–807. https://doi.org/10.1097/JTO.0b013e318248240b.
50. Zhou, Z., Hao, Y., Liu, N., Raptis, L., Tsao, M.S., and Yang, X. (2011). TAZ is a novel oncogene in non-small cell lung cancer. Oncogene *30*, 2181–2186. https://doi.org/10.1038/onc.2010.606.
51. Li, Z., Wang, Y., Zhu, Y., Yuan, C., Wang, D., Zhang, W., Qi, B., Qiu, J., Song, X., Ye, J., et al. (2015). The Hippo transducer TAZ promotes epithelial to mesenchymal transition and cancer stem cell maintenance in oral cancer. Mol. Oncol. *9*, 1091–1105. https://doi.org/10.1016/j.molonc.2015.01.007.
52. Lamar, J.M., Xiao, Y., Norton, E., Jiang, Z.G., Gerhard, G.M., Kooner, S., Warren, J.S.A., and Hynes, R.O. (2019). SRC tyrosine kinase activates the YAP/TAZ axis and thereby drives tumor growth and metastasis. J. Biol. Chem. *294*, 2302–2317. https://doi.org/10.1074/jbc.RA118.004364.
53. Dupont, S., Morsut, L., Aragona, M., Enzo, E., Giulitti, S., Cordenonsi, M., Zanconato, F., Le Digabel, J., Forcato, M., Bicciato, S., et al. (2011). Role of YAP/TAZ in mechanotransduction. Nature *474*, 179–183. https://doi.org/10.1038/nature10137.
54. Khalil, A.A., Smits, D., Haughton, P.D., Koorman, T., Jansen, K.A., Verhagen, M.P., van der Net, M., van Zwieten, K., Enserink, L., Jansen, L., et al. (2024). A YAP-centered mechanotransduction loop drives collective breast cancer cell invasion. Nat. Commun. *15*, 4866. https://doi.org/10.1038/s41467-024-49230-z.
55. Zhang, J., Goliwas, K.F., Wang, W., Taufalele, P.V., Bordeleau, F., and Reinhart-King, C.A. (2019). Energetic regulation of coordinated leader-follower dynamics during collective invasion of breast cancer cells. Proc. Natl. Acad. Sci. USA *116*, 7867–7872. https://doi.org/10.1073/pnas.1809964116.
56. Bernstein, B.W., and Bamburg, J.R. (2003). Actin-ATP hydrolysis is a major energy drain for neurons. J. Neurosci. *23*, 1–6. https://doi.org/10.1523/JNEUROSCI.23-01-00002.2003.
57. Richardson, A.M., Havel, L.S., Koyen, A.E., Konen, J.M., Shupe, J., Wiles, W.G., 4th, Martin, W.D., Grossniklaus, H.E., Sica, G., Gilbert-Ross, M., and Marcus, A.I. (2018). Vimentin Is Required for Lung Adenocarcinoma Metastasis via Heterotypic Tumor Cell-Cancer-Associated Fibroblast Interactions during Collective Invasion. Clin. Cancer Res. *24*, 420–432. https://doi.org/10.1158/1078-0432.CCR-17-1776.
58. Bronsert, P., Enderle-Ammour, K., Bader, M., Timme, S., Kuehs, M., Csanadi, A., Kayser, G., Kohler, I., Bausch, D., Hoeppner, J., et al. (2014). Cancer cell invasion and EMT marker expression: a three-dimensional study of the human cancer-host interface. J. Pathol. *234*, 410–422. https://doi.org/10.1002/path.4416.
59. Zhang, X., Liu, G., Kang, Y., Dong, Z., Qian, Q., and Ma, X. (2013). N-cadherin expression is associated with acquisition of EMT phenotype and with enhanced invasion in erlotinib-resistant lung cancer cell lines. PLoS One *8*, e57692. https://doi.org/10.1371/journal.pone.0057692.
60. Jia, D., Yan, M., Wang, X., Hao, X., Liang, L., Liu, L., Kong, H., He, X., Li, J., and Yao, M. (2010). Development of a highly metastatic model that reveals a crucial role of fibronectin in lung cancer cell migration and invasion. BMC Cancer *10*, 364. https://doi.org/10.1186/1471-2407-10-364.
61. Bushweller, J.H. (2019). Targeting transcription factors in cancer — from undruggable to reality. Nat. Rev. Cancer *19*, 611–624. https://doi.org/10.1038/s41568-019-0196-7.
62. Liu-Chittenden, Y., Huang, B., Shim, J.S., Chen, Q., Lee, S.J., Anders, R.A., Liu, J.O., and Pan, D. (2012). Genetic and pharmacological disruption of the TEAD-YAP complex suppresses the oncogenic activity of YAP. Genes Dev. *26*, 1300–1305. https://doi.org/10.1101/gad.192856.112.
63. Wang, C., Zhu, X., Feng, W., Yu, Y., Jeong, K., Guo, W., Lu, Y., and Mills, G.B. (2016). Verteporfin inhibits YAP function through up-regulating 14-3-3σ sequestering YAP in the cytoplasm. Am. J. Cancer Res. *6*, 27–37.
64. Baroja, I., Kyriakidis, N.C., Halder, G., and Moya, I.M. (2024). Expected and unexpected effects after systemic inhibition of Hippo transcriptional output in cancer. Nat. Commun. *15*, 2700. https://doi.org/10.1038/s41467-024-46531-1.
65. Yan, F., Qian, M., He, Q., Zhu, H., and Yang, B. (2020). The posttranslational modifications of Hippo-YAP pathway in cancer. Biochim. Biophys. Acta Gen. Subj. *1864*, 129397. https://doi.org/10.1016/j.bbagen.2019.07.006.
66. Hata, S., Hirayama, J., Kajiho, H., Nakagawa, K., Hata, Y., Katada, T., Furutani-Seiki, M., and Nishina, H. (2012). A novel acetylation cycle of transcription co-activator Yes-associated protein that is downstream of Hippo pathway is triggered in response to SN2 alkylating agents. J. Biol. Chem. *287*, 22089–22098. https://doi.org/10.1074/jbc.M111.334714.
67. Peng, C., Zhu, Y., Zhang, W., Liao, Q., Chen, Y., Zhao, X., Guo, Q., Shen, P., Zhen, B., Qian, X., et al. (2017). Regulation of the Hippo-YAP Pathway by Glucose Sensor O-GlcNAcylation. Mol. Cell *68*, 591–604.e5. https://doi.org/10.1016/j.molcel.2017.10.010.
68. Zhang, X., Qiao, Y., Wu, Q., Chen, Y., Zou, S., Liu, X., Zhu, G., Zhao, Y., Chen, Y., Yu, Y., et al. (2017). The essential role of YAP O-GlcNAcylation in high-glucose-stimulated liver tumorigenesis. Nat. Commun. *8*, 15280. https://doi.org/10.1038/ncomms15280.
69. Hsu, P.C., Yang, C.T., Jablons, D.M., and You, L. (2020). The Crosstalk between Src and Hippo/YAP Signaling Pathways in Non-Small Cell Lung Cancer (NSCLC). Cancers *12*, 1361. https://doi.org/10.3390/cancers12061361.
70. Zhao, B., Li, L., Tumaneng, K., Wang, C.Y., and Guan, K.L. (2010). A coordinated phosphorylation by Lats and CK1 regulates YAP stability through SCF(beta-TRCP). Genes Dev. *24*, 72–85. https://doi.org/10.1101/gad.1843810.
71. He, X., Riceberg, J., Soucy, T., Koenig, E., Minissale, J., Gallery, M., Bernard, H., Yang, X., Liao, H., Rabino, C., et al. (2017). Probing the roles of SUMOylation in cancer cell biology by using a selective SAE inhibitor. Nat. Chem. Biol. *13*, 1164–1171. https://doi.org/10.1038/nchembio.2463.
72. Lightcap, E.S., Yu, P., Grossman, S., Song, K., Khattar, M., Xega, K., He, X., Gavin, J.M., Imaichi, H., Garnsey, J.J., et al. (2021). A small-molecule SUMOylation inhibitor activates antitumor immune responses and potentiates immune therapies in preclinical models. Sci. Transl. Med. *13*, eaba7791. https://doi.org/10.1126/scitranslmed.aba7791.
73. Zhang, Z., Du, J., Wang, S., Shao, L., Jin, K., Li, F., Wei, B., Ding, W., Fu, P., van Dam, H., et al. (2019). OTUB2 Promotes Cancer Metastasis via Hippo-Independent Activation of YAP and TAZ. Mol. Cell *73*, 7–21.e7. https://doi.org/10.1016/j.molcel.2018.10.030.
74. Song, S., Honjo, S., Jin, J., Chang, S.S., Scott, A.W., Chen, Q., Kalhor, N., Correa, A.M., Hofstetter, W.L., Albarracin, C.T., et al. (2015). The Hippo Coactivator YAP1 Mediates EGFR Overexpression and Confers Chemoresistance in Esophageal Cancer. Clin. Cancer Res. *21*, 2580–2590. https://doi.org/10.1158/1078-0432.CCR-14-2191.
75. Noguchi, S., Saito, A., Horie, M., Mikami, Y., Suzuki, H.I., Morishita, Y., Ohshima, M., Abiko, Y., Mattsson, J.S.M., König, H., et al. (2014). An integrative analysis of the tumorigenic role of TAZ in human non-small cell lung cancer. Clin. Cancer Res. *20*, 4660–4672. https://doi.org/10.1158/1078-0432.CCR-13-3328.
76. Yang, N., Morrison, C.D., Liu, P., Miecznikowski, J., Bshara, W., Han, S., Zhu, Q., Omilian, A.R., Li, X., and Zhang, J. (2012). TAZ induces growth factor-independent proliferation through activation of EGFR ligand amphiregulin. Cell Cycle *11*, 2922–2930. https://doi.org/10.4161/cc.21386.
77. Nan, X., Xie, C., Yu, X., and Liu, J. (2017). EGFR TKI as first-line treatment for patients with advanced EGFR mutation-positive non-small-cell lung cancer. Oncotarget *8*, 75712–75726. https://doi.org/10.18632/oncotarget.20095.
78. Li, Y., Zang, H., Qian, G., Owonikoko, T.K., Ramalingam, S.R., and Sun, S.Y. (2020). ERK inhibition effectively overcomes acquired resistance of epidermal growth factor receptor-mutant non-small cell lung cancer cells to osimertinib. Cancer *126*, 1339–1350. https://doi.org/10.1002/cncr.32655.
79. Schindelin, J., Arganda-Carreras, I., Frise, E., Kaynig, V., Longair, M., Pietzsch, T., Preibisch, S., Rueden, C., Saalfeld, S., Schmid, B., et al. (2012). Fiji: an open-source platform for biological-image analysis. Nat. Methods *9*, 676–682. https://doi.org/10.1038/nmeth.2019.
80. Philip, P.A., Azar, I., Xiu, J., Hall, M.J., Hendifar, A.E., Lou, E., Hwang, J.J., Gong, J., Feldman, R., Ellis, M., et al. (2022). Molecular Characterization of KRAS Wild-type Tumors in Patients with Pancreatic Adenocarcinoma. Clin. Cancer Res. *28*, 2704–2714. https://doi.org/10.1158/1078-0432.CCR-21-3581.

STAR★METHODS

KEY RESOURCES TABLE

REAGENT or RESOURCE	SOURCE	IDENTIFIER
Antibodies		
YAP (WB, IF)	Cell Signaling Technology	Cat#14074; RRID: AB_2650491
TAZ (WB, IHC, IF)	Cell Signaling Technology	Cat#4883; RRID: AB_1904158
TEAD1	Cell Signaling Technology	Cat#12292; RRID: AB_2797873
S6	Cell Signaling Technology	Cat#2317; RRID: AB_2238583
pS6	Cell Signaling Technology	Cat#4858; RRID: AB_916156
Zeb1	Cell Signaling Technology	Cat#70512; RRID: AB_2935802
CTGF	Cell Signaling Technology	Cat#86641; RRID: AB_2800085
EGFR	Cell Signaling Technology	Cat#4267; RRID: AB_2246311
pAKT	Cell Signaling Technology	Cat#4060; RRID: AB_2315049
AKT	Cell Signaling Technology	Cat#4691; RRID: AB_915783
βTrCP	Cell Signaling Technology	Cat#4394; RRID: AB_10545763
pGSK3-β	Cell Signaling Technology	Cat#9336; RRID: AB_331405
GSK	Cell Signaling Technology	Cat#12456; RRID: AB_2636978
SUMO-1	Cell Signaling Technology	Cat#4940; RRID: AB_2302825
actin	Cell Signaling Technology	Cat#3700; RRID: AB_2242334
N-cadherin	BD Biosciences	Cat#610920; RRID: AB_2077527
Fibronectin	Abcam	Cat#ab2413; RRID: AB_2262874
YAP (IHC, IP, IF)	Cell Signaling Technology	Cat#12395; RRID: AB_2797897
TAZ (IP)	Abcam	Cat#ab242313
Alexa Fluor™ 568 goat anti-rabbit	Invitrogen	Cat#A11011; RRID: AB_143157
Alexa Fluor™ 635 goat anti-mouse	Invitrogen	Cat#A31574; RRID: AB_2536184
Alexa Fluor™ 594 goat anti-rabbit	Invitrogen	Cat#A32740; RRID: AB_2762824
Alexa Fluor™ 488 goat anti-mouse	Invitrogen	Cat#A32723; RRID: AB_2633275
Bacterial strain		
Stable Competent E. Coli	NEW ENGLAND Biolabs	C3040I
Biological sample		
Human lung cancer tissue microarray	TissueArray.Com	LC817b
Chemicals, peptides, and recombinant proteins		
Erlotinib	Selleckchem	Cat#S7786
Matrigel Basement Membrane Matrix	Corning	Cat#356237
jetPRIME Polyplus transfection reagent	Polypus	Cat#114-07
Polybrene Transfection Reagent	Sigma-Aldrich	Cat# TR-1003-G
RPMI 1640	Corning	Cat#10-040-CV
Puromycin	Thermo Scientific	Cat#AAJ67236-8EQ
4–20% Mini-PROTEAN® TGX Stain-Free™ Protein Gels	Bio-Rad	Cat#4568096
4–20% Mini-PROTEAN® TGX Stain-Free™ Protein Gels	Bio-Rad	Cat#4568093
Bio-Rad Protein Assay Dye Reagent Concentrate	Bio-Rad	Cat#5000006
Live dead stain	Invitrogen	Cat#S34859
(2-Hydroxypropyl)-β-cyclodextrin	Sigma	Cat#H107
PVDF membrane	Millipore	Cat#IPVH00010

(*Continued on next page*)

Continued

REAGENT or RESOURCE	SOURCE	IDENTIFIER
DAPI	Thermo Scientific	Cat#D1306
Fixation buffer	Biolegend	Cat#420801
Intracellular staining perm wash buffer	Biolegend	Cat#421002
Prolong gold mounting media	Thermo Scientific	Cat#P10144
N-Ethylmaleimide	Sigma	Cat#S3692
Protein G Agarose	Millipore	Cat#16-266
RIPA Buffer	Sigma	Cat#R0278
BLOK Casein in TBS	G-Biosciences	Cat#786-196
AKT inhibitor VIII	MedChemExpress	Cat#HY-10355
EGF recombinant protein	Thermo Scientific	Cat#AF-100-15
TAK-981	MedChemExpress	Cat#HY-111789
Critical commercial assays		
CellTiter-Glo assay	Promega	Cat# G9248
CellTiter-Glo 3D	Promega	Cat#G9681
GeneJET RNA Purification Kit	Thermo Scientific	Cat#K0732
RevertAid First Strand cDNA Synthesis Kit	Thermo Scientific	Cat#K1622
DyNAmo ColorFlash probe quantitative polymerase chain reaction (PCR) kit	Thermo Scientific	Cat#F456S
NE-PER Nuclear and Cytoplasmic Extraction Reagents	Thermo Scientific	Cat#78833
ImmPRESS HRP Reagent Kit	VectorLabs	MP-7401
ImmPACT DAB Peroxidase Substrate Kit	VectorLabs	SK4105
Experimental models: Cell lines		
Human:H1299-leader cells	Commander et al.[20]	N/A
Human:H1299-follower cells	Commander et al.[20]	N/A
Human:H1299	Commander et al.[20]	N/A
Human:H460	Adam Marcus, Emory University	N/A
Human:H23	Adam Marcus, Emory University	N/A
Human:H1975	Adam Marcus, Emory University	N/A
Human:H596	Adam Marcus, Emory University	N/A
Human:PC9	Sun et al.[78]	N/A
Human:A549	ATCC	Cat#CCL-185
Human:H293T	ATCC	Cat#CRL-3216
Experimental models: Organisms/strains		
NOD scid gamma NSG™	Jackson Laboratory	Cat#006667
Oligonucleotides		
shRNA targeting sequence TAZ#1; TAAGCTTTATGGGTGTTAATT	Merck	Cat#TRCN000370006
shRNA targeting sequence TAZ#2; CAGCCAAATCTCGTGATGAAT	Merck	Cat#TRCN000319150
shRNA targeting sequence YAP#1; CAGGTGATACTATCAACCAAA	Merck	Cat#TRCN000107267
shRNA targeting sequence YAP#2; CAGGTGATACTATCAACCAAA	Merck	Cat#TRCN000107267

(*Continued on next page*)

Continued

REAGENT or RESOURCE	SOURCE	IDENTIFIER
shRNA targeting sequence βTrCP#1; GCACATAAACTCGTATCTTAA	Merck	Cat#TRCN0000006542
shRNA targeting sequence βTrCP#2; GCGTTGTATTCGATTTGATAA	Merck	Cat#TRCN0000006543
EGFR Taqman™ assay probe	Thermo Scientific	Cat#Hs01076078_m1
YAP Taqman™ assay probe	Thermo Scientific	Cat#Hs00902712_g1
TAZ Taqman™ assay probe	Thermo Scientific	Cat#Hs00210007_m1
Smurf2 Taqman™ assay probe	Thermo Scientific	Cat#Hs00224203_m1
MARCH4 Taqman™ assay probe	Thermo Scientific	Cat#Hs00863129_m1
DTX3 Taqman™ assay probe	Thermo Scientific	Cat#Hs01595350_m1
LONRF3 Taqman™ assay probe	Thermo Scientific	Cat#Hs00983071_m1
MID1 Taqman™ assay probe	Thermo Scientific	Cat#Hs00931793_m1
TRIM38 Taqman™ assay probe	Thermo Scientific	Cat#Hs00197164_m1
TRIM8 Taqman™ assay probe	Thermo Scientific	Cat#Hs00229451_m1
TRIM6 Taqman™ assay probe	Thermo Scientific	Cat#Hs04194831_s1
Recombinant DNA		
pLVX-IRES-Neo	Takara	Cat#632181
HA-AKT1-pLVX-IRES-Neo	This paper	N/A
Flag-AKT2-pLVX-IRES-Neo	This paper	N/A
Flag-TrCP-pLVX-IRES-Neo	This paper	N/A
EGFP-TAZ-pLVX-IRES-Neo	This paper	N/A
mCherry-YAP-pLVX-IRES-Neo	This paper	N/A
Software and algorithms		
Fiji software	Schindelin et al.[79]	
GraphPad Prism software	GraphPad Software	http://www.graphpad.com
Biorender	Science Suite Inc.	https://www.biorender.com
Adobe Illustrator	Adobe Inc	https://www.adobe.com/products/illustrator.html

EXPERIMENTAL MODEL AND STUDY PARTICIPANT DETAILS

In vivo animal studies

Animal experiments were conducted according to protocols approved by Emory University's Institutional Animal Care and Use Committee (IACUC). 9-week-old Male NSG™ mouse (body weight 27±2 g) obtained from Jackson Laboratories were used for animal experiments. Formalin-fixed paraffin-embedded tumors from lung cancer patients were obtained from TissueArray.com.

Cell lines

Leader and follower cells derived from H1299 and H1299, H460, H23, H1975, H596 lung cancer cell lines were obtained from Dr. Adam Marcus, Winship Cancer Institute, Emory University. A549 and Human embryonic kidney (HEK) 293T cells were obtained from the American Type Culture Collection (ATCC). PC9 was obtained from Dr. Shi-Yong Sun, Winship Cancer Institute, Emory University. Follower and leader low passage cells were used for these experiments with validation of their identity by interrogating fibronectin expression.[7]

Cell culture

NSCLC lines were cultured in complete RPMI 1640 with 10% fetal bovine serum (FBS). HEK293T cells were cultured in Dulbecco's modified Eagle's medium (Gibco) with 10% FBS and penicillin (100 U/ml)/ streptomycin (100 μg/ml) and maintained in a 37°C incubator with 5% CO2.

METHOD DETAILS

Generation of shRNA KDs

shRNA bacterial stocks were obtained from Sigma-Aldrich and plated on LB agar plates containing ampicillin. Plasmids purified from ampicillin-resistant colonies were transfected into HEK293T using jetPRIME Polyplus transfection reagent. Medium was changed after 4 h, and then incubated for 72 h to allow for virus production. The supernatant was collected and filtered using a 0.45 μm filter. Leader and follower cells were transduced with lentiviral particles using a standard transduction protocol. Briefly, $1.5x10^4$ leader and follower cells were seeded in a 6-well plate in complete RPMI media. The following day, 500 μl of virus and Polybrene Infection/Transfection Reagent was added to a final concentration of 8 ug/ml. Spinfection was performed by centrifugation at 2500 rpm at room temperature for 30 minutes followed by a media replacement (with complete media) after 24 h. Puromycin (0.5 μg/ml for leader cells and 2 μg/ml for follower cells) was added the following day and cultures selected for 7 days.

Reverse transcription quantitative polymerase chain reaction

Reagents/probes used are as listed: Thermo Scientific GeneJET RNA Purification Kit used for RNA isolation; cDNA synthesis, Thermo Scientific RevertAid First Strand cDNA Synthesis Kit ; Thermo Scientific DyNAmo ColorFlash probe quantitative polymerase chain reaction (PCR) kit; Bio-Rad S1000 Thermal Cycler and TaqMan probes with Applied Biosystems 7500 Real-Time PCR system.

Immunoblotting

Cells were harvested and washed twice with phosphate-buffered saline (PBS) and whole-cell lysates prepared with radioimmunoprecipitation assay (RIPA) buffer supplemented with phosphatase and protease inhibitors and 1% phenylmethylsulfonyl fluoride (PMSF) following 20 min on ice. Cell debris was removed by centrifugation at 14,000 rpm at 4°C for 15 min. Total protein concentration was determined using Bio-Rad Protein Assay Dye Reagent Concentrate. Samples were normalized to a total protein concentration of 20 to 30 μg in 1× Laemmli buffer containing β-mercaptoethanol and boiled for 10 min at 95°C followed by resolution by SDS–polyacrylamide gel electrophoresis. Proteins were transferred to polyvinylidene fluoride (PVDF) membrane. PVDF membranes were incubated in blocking solution [5% milk in tris-buffered saline (TBS) with Tween 20] for 1 hour, followed by washing and incubation with primary antibodies [1:1000 dilution or as suggested by the manufacturer in BLOK Casein in TBS] overnight. After washing, secondary antibodies were added at a dilution of 3:10,000 in blocking solution for 1 hour. Nuclear and cytoplasmic extracts were prepared as per manufacturer's instructions using NE-PER™ kit.

Cell viability/proliferation assays

CellTiter-Glo assay was performed using 2000 cells per 100 microliters plated in triplicates in 96-well white flat-bottom plates. One hundred microliters of CellTiter-Glo assay reagent was added to each well, followed by a 10 min incubation at room temperature. ATP levels were assessed using a BioTek SYNERGY H1 microplate reader following the manufacturer's instructions. Proliferation in 3D culture was measured using CellTiter-Glo 3D as per manufacturer's instructions with relative luminescence units (RLU) plotted. Live dead stain was used to analyze cell viability as per the manufacturer's instructions using a Cytek Aurora flow cytometer and analyzed with the *De Novo* Software FCS Express version 4.

Live cell oxygen consumption and extracellular acidification rates

Oxygen consumption rate and extracellular acidification rates were measured using Seahorse bioscience extracellular flux (XFe96) analyzer. The Agilent Seahorse XF Cell Mito Stress Test was performed. In brief, leader or follower cells were seeded at a density of 20,000 cells per well of an XF 24 well cell culture microplate and incubated overnight to ensure attachment. Before the assay, cells were equilibrated in buffered (pH 7.4) Seahorse XF base medium supplemented with 10 mM glucose, 1 mM sodium pyruvate, and 2 mM glutamine in a non-CO2 incubator. Cellular metabolism was examined through sequential injections of oligomycin (2.5 μM), carbonyl cyanide 4- (trifluoromethoxy) phenylhydrazone (FCCP, 0.5 μM) and rotenone (2 μM)/ antimycin A (2 μM). Basal respiration rate was calculated as baseline OCR subtracted by the OCR after the injection of antimycin and rotenone.

Spheroid formation and invasion assays

Spheroids were formed by seeding 3000-5000 leader and follower cells/well in ultra-low attachment 96-well round bottom plates. After spheroid formation in round bottom plates, the spheroids were embedded within the recombinant basement matrix (Matrigel) in a 35 mm glass bottom dish with a 14 mm microwell where the bottom surface is with a No. 1.5 coverglass (Mattek P35G-1.5-14-C) for imaging purposes and allowed to invade and traffic along the interface between the glass coverslip and the 3D matrix for up to 72 h at 37°C. For drug treatments, compounds were added directly to the matrigel during the embedding process, as well as to the growth media. Images of the spheroids were taken using an Olympus IX51 microscope (4X magnification and 0.30 NA) with an Infinity2 CCD camera. Invasive area was quantified on the 2D images by measuring both the total spheroid area around the outer perimeter and the inner spheroid core in ImageJ/Fiji and calculating the difference between the two measures.

Scratch assay

$0.12x10^6$ follower cells and $0.18 x10^6$ leader cells per well were seeded in 12-well plates. When cells were approximately 90-100% confluent, a scratch was introduced with a 200μL pipette tip. Gap closure was imaged at 0 and 24 h with Olympus IX51 microscope 10X magnification, capturing at least 4 fields for each condition. The migration distance was assessed manually using image J software (National Institutes of Health, USA). Gap closure was calculated using the following formula: (0hr gap width-24 h gap width)/0hr gap width.

In vivo mouse studies

H1299 cells obtained from Adam Marcus, Winship Cancer Institute, Emory University were injected into NSG™. H1299 derived allograft experiments were approved by the Institutional Animal Care and Use Committee (IACUC) of Emory University (PROTO201700269). $1X10^6$ H1299 cells suspended in 100 μL PBS were introduced by subcutaneous injection in the right flank. When tumors were palpable, approximately 3 weeks after injection of tumor cells, treatments were started. Intraperitoneal injection of 0.2 mL of 25 mg/kg TAK- 981 suspended in 20% HPBCD (Sigma), pH 6-7 or vehicle control were performed thrice weekly. Tumor volume, and body weight were measured twice a week using a digital vernier caliper, until the end point of the experiment. The mean tumor volume was calculated using the formula: volume (V)= L X W X W X 0.5, where W and L are the width and length of the tumor, respectively. Mice were euthanized according to IACUC guidelines and necropsied at 45 day. Tumor and lung tissues were isolated.

Immunohistochemistry (IHC) staining

Lung cancer tissue samples were obtained from TissueArray.Com. Slides were deparaffinized with antigen retrieval performed using Antigen Unmasking Solution. BlockALL Blocking solution was applied for blocking endogenous peroxidase. Immunohistochemistry staining was performed using anti-TAZ antibody (1:600), anti-YAP antibody (1:600). ImmPRESS HRP Reagent Kit and ImmPACT DAB Peroxidase Substrate Kit were used for detection per manufacturer's instructions. Brightfield images were captured using Keyence BZ-X 810 and DAB staining intensities were quantified using ImageJ. H&E sections of lung and liver were evaluated for presence of micro and macro metastases. Micro metastases were defined as clusters of less than 10 cells, including individual cells. Macro metastases were defined as clusters of greater than 10 cells.

Immunofluorescence and confocal microscopy

Leader and follower cells were seeded onto coverslips. Next day, after 2 PBS washes, cells were fixed with fixation buffer. Cover slips were washed thrice with 1X PBS and then blocked with 4% BSA prepared in intracellular staining perm wash buffer for 1 h, followed by overnight incubation with primary antibody YAP (1:500) and TAZ (1:500) prepared in perm wash buffer at 4°C. Subsequently, cells were washed with perm wash buffer and stained with Alexa Fluor 568 and 635 conjugated secondary antibody prepared in perm wash buffer for 1 h at RT. After PBS wash, DAPI was added for nuclear staining followed by mounting of coverslips with prolong gold mounting media. Micrographs were captured using confocal Leica SP8 at 60X magnification and zoom factor of 1.5.

H1299 3D spheroids were fixed using fixation buffer for 40 min at RT. After 2 PBS washes, the spheroids were blocked for 1 h with 2% BSA prepared in intracellular staining perm wash buffer. This was followed by an overnight incubation at RT with primary antibodies; rabbit TAZ (1:300), YAP (1:300), and mouse N-Cadherin (1:300) prepared in perm wash buffer with 2% BSA. Following a wash with perm wash buffer, the spheroids were stained for 1 h at RT with Alexa Fluor 594 and 488 conjugated secondary antibodies against rabbit and mouse, respectively, in perm wash buffer. After a PBS wash, DAPI was used for nuclear staining, followed by a 10 min PBS wash. The 3D invading spheroids were imaged using confocal Nikon Crest Optics SD at 20X and 40X magnification.

Coimmunoprecipitation

Cells were washed once with PBS and lysed in RIPA buffer containing 20 mM N-ethylmaleimide, protease and phosphatase inhibitors and PMSF for 30 min on ice. Debris was removed by centrifugation at 14,000 rpm at 4°C for 15 min. Total protein concentration was determined using Bio-Rad Protein Assay Dye Reagent Concentrate. 400μL lysates containing 200 μg protein were precleared by incubating for 1 h at 4°C with 50 μL of Protein G Agarose, prewashed with PBS. Precleared lysates were collected by centrifugation at 5000 rpm for 2 min at 4°C and incubated with rotation overnight at 4°C with 50 μL of Protein G Agarose, preincubated with 5 μL of TAZ and YAP antibody overnight. Pelleted matrix was washed twice with 500 μL ice-cold PBS, and proteins were eluted after boiling at 95°C for 5 min in 30 μL of 2× electrophoresis sample buffer containing β-mercaptoethanol.

Bioinformatics analysis

The Winship Molecular profiling study (2020) conducted in partnership with Caris life Sciences was used to perform correlation analyses.[80] Log2 transformed data were normalized and a Spearman correlation analysis performed to determine *p* value (two-tailed) for the above studies. This institutional dataset was downloaded from cBioPortal (https://cbioportal.winship.emory.edu/) for *n*=343 LUAD patients (accessed on 06/01/2023). The cohort contained samples from NSCLC patients who have been treated with various therapy including drugs for immunotherapy such as pembrolizumab (Keytruda), nivolumab/ipilimumab combination and targeted therapy with EGFR inhibitors such as osimertinib and gefitinib. Bioinformatics analysis: TCGA- Firehose legacy LUAD cohort (*n=365*) protein expression dataset was

downloaded from cbioportal (https://www.cbioportal.org/). Pearson correlation analysis (p-value (two-tailed) ≤ 0.05) was performed using Graphpad prism software, version 9. Clinicopathological features of the dataset are described in Tables S1 and S2.

QUANTIFICATION AND STATISTICAL ANALYSIS

Graphical presentation and statistical analysis were performed using GraphPad Prism 9.0. Statistical analysis of significance was based on unpaired two-tailed Student's t test and one -way ANOVA followed by Tukey post hoc test for all figures and Pearson's r for Figure 2. Data with error bars represent mean $\pm$ standard error of the mean (SEM). The number of experimental replicates is listed in each figure panel. Statistical analyses were performed based on the homogeneity of variances and assumptions of normal distribution. p values of less than 0.05 were considered statistically significant.